CHALMERS
UNIVERSITY OF TECHNOLOGY

LICENTIATE THESIS

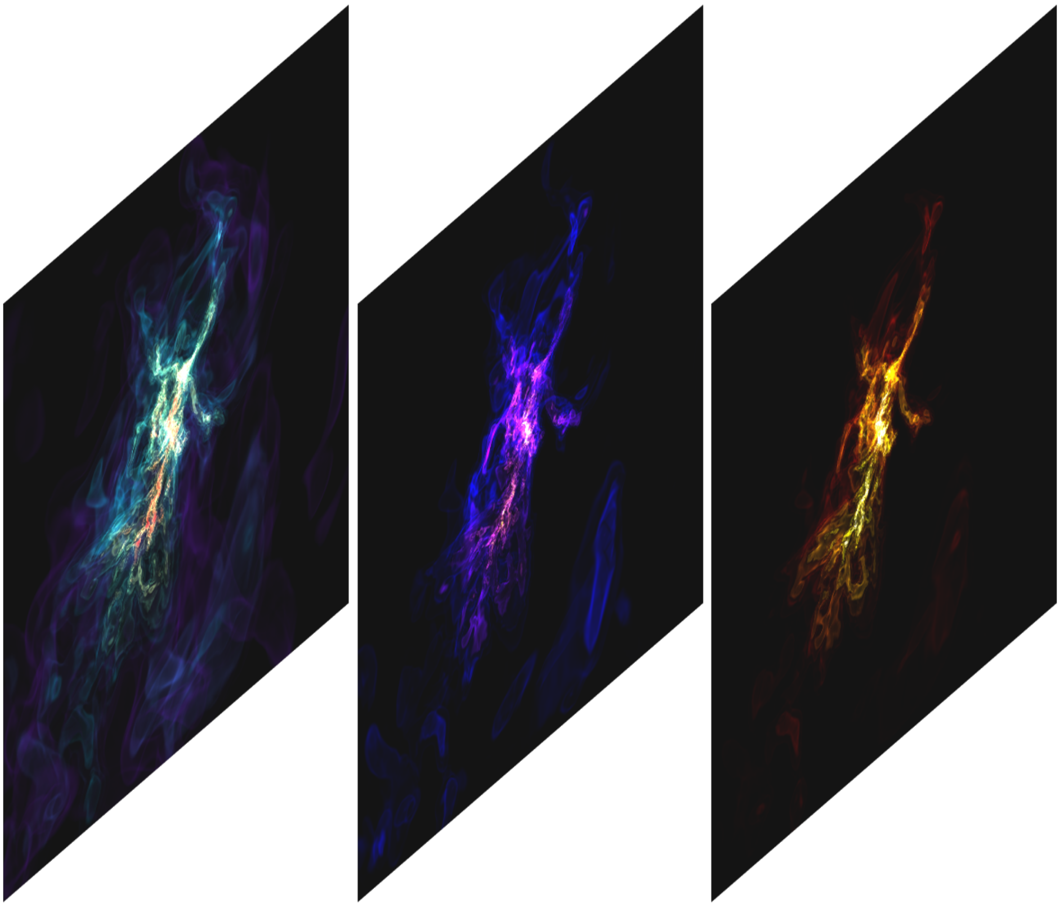

# Chemodynamics in Star-Forming Molecular Clouds

CHIA-JUNG HSU

*Department of Space, Earth, and Environment*
CHALMERS UNIVERSITY OF TECHNOLOGY
Gothenburg, Sweden 2021

Thesis for the degree of Licentiate of Philosophy

# Chemodynamics in Star-Forming Molecular Clouds

Chia-Jung Hsu

Department of Space, Earth, and Environment
CHALMERS UNIVERSITY OF TECHNOLOGY
Göteborg, Sweden 2021

Chemodynamics in Star-Forming Molecular Clouds
CHIA-JUNG HSU

© CHIA-JUNG HSU, 2021.

Division of Astronomy & Plasma Physics
Department of Space, Earth, and Environment
Chalmers University of Technology
SE–412 96 Göteborg, Sweden
Telephone + 46 (0) 31 – 772 1000

Cover: Volume rendering of a simulated fast collapsing massive prestellar core at 60.8 kyr. Left: density, Middle: number density of $N_2H^+$, Right: number density of $N_2D^+$. The details are described in Paper I.

Typeset by the author using LaTeX.

Printed by Chalmers Reproservice
Göteborg, Sweden 2021

*hope everyone stays safe during the covid-19 pandemic*

# Abstract

Stars are fundamental building blocks of galaxies. However, the answers to many basic questions about their formation remain elusive. There is no consensus on a theory that can predict the rate of star formation, its clustering properties, and the conditions needed for massive stars to be born. Although stars are known to form from dense regions of molecular clouds, measuring the physical properties in such regions is an outstanding challenge. Astrochemistry is the crucial set of processes that control the chemical evolution of the universe. It is important for controlling physical evolution, e.g., by setting heating and cooling rates and ionization fractions, but also for allowing predictions to be made for the emission from key diagnostic species to probe interstellar processes, such as star formation. To reconstruct the three-dimensional structures of galaxies and their interstellar media, chemodynamics, which is the combination of hydrodynamics and chemistry, is necessary.

In this thesis, chemodynamical simulations are applied to star-forming regions to follow their combined physical and chemical evolution and make predictions for observations. In particular a gas phase deuterium fractionation network is applied to massive prestellar core simulations. Various chemical model parameters are investigated to understand whether fast collapse of a turbulent, magnetised prestellar core can achieve the high levels of deuteration that are commonly observed in such systems. The structure, kinematics and dynamics of the core, as traced by the rotational transitions of the key diagnostic species of $N_2D^+$, are investigated. Another astrochemical network, including gas-grain processes, is constructed for simulations of larger-scale, generally lower density molecular clouds and applied to a simulation of giant molecular cloud collisions. We also discuss the computational performance of our chemodynamical simulations and summarize some methods to improve their efficiency.

**Keywords:** astrochemistry, hydrodynamics, methods: numerical, stars: formation, ISM: clouds

# Acknowledgments

First, I would like to thank my supervisor, Jonathan Tan, for his support and patience. His insightful and valuable suggestions always lead me on the right way to accomplish things step by step. I also appreciate him giving me the opportunity to work on Astrochemistry and Chemodynamics with Paola Caselli, Serena Viti, and other collaborators. I am so grateful to receive a lot of precious comments and experiences from them. Special thanks to my examiner, Susanne Aalto, for agreeing to take the place in an accidental situation.

Many thanks to Camilla, Juan, Sandra, and my office mate (although we sadly moved out of the office), Andri, for helping me move and get used to the life in Sweden. Moving to a new country is always a big challenge. Thanks to all the people at SEE Department for creating an enjoyable working environment. Thanks to all Taiwanese friends in Gothenburg for helping me overcome homesickness. Finally, special thanks to my family for their support and encouragement.

Chia-Jung Hsu
Göteborg, February 2021

# List of Publications

This thesis is based on the following appended papers:

**Paper 1.** Chia-Jung Hsu, Jonathan C. Tan, Matthew D. Goodson, Paola Caselli, Bastian Körtgen, Yu Cheng *Deuterium Chemodynamics of Massive Pre-stellar Cores* Accepted by MNRAS (2020).

# Contents

**Abstract** **v**

**Acknowledgments** **vii**

**List of Publications** **ix**

## I Introductory chapters 1

**1 General Introduction** **3**
1.1 Interstellar Medium, Star Formation and Massive Star Formation . . 3
1.2 Virial Theorem . . . . . . . . . . . . . . . . . . . . . . . . . . . . . . 5
1.3 Magnetic Fields and Mass-to-Flux Ratio . . . . . . . . . . . . . . . . 5

**2 Astrochemical Modeling** **7**
2.1 Deuterium Fractionation . . . . . . . . . . . . . . . . . . . . . . . . . 7
2.2 UCLCHEM . . . . . . . . . . . . . . . . . . . . . . . . . . . . . . . . 10

**3 Chemodynamics Simulations** **15**
3.1 Coupling Chemistry with Magnetohydrodynamics . . . . . . . . . . . 15
3.2 Simulation Code: `ENZO+KROME` . . . . . . . . . . . . . . . . . . . . 17
3.3 Performance . . . . . . . . . . . . . . . . . . . . . . . . . . . . . . . 17

**4 Introduction to Paper** **21**
4.1 Paper I . . . . . . . . . . . . . . . . . . . . . . . . . . . . . . . . . . 21

**5 Outlook and Future Work** **23**
5.1 Ambipolar Diffusion in Massive PSCs . . . . . . . . . . . . . . . . . . 23
5.2 Cloud-Cloud Collisions . . . . . . . . . . . . . . . . . . . . . . . . . . 27
5.3 Porting astrochemical tools onto GPUs . . . . . . . . . . . . . . . . . 27

**Bibliography** **31**

## II Appended papers 37

**1 Deuterium Chemodynamics of Massive Pre-stellar Cores** **39**

# Part I

# Introductory chapters

# Chapter 1

# General Introduction

Stars are fundamental objects of the universe. However, there is no settled theory for describing how, where and with what frequency star formation occurs. As the material pervading the space between stars, the interstellar medium (ISM) has a directly connection and contribution to star formation. In the course of the evolution of a galaxy, the interstellar medium is gradually converted into stars. As the stars evolve, and especially at the end of their lives, they return some of their matter back to the ISM, e.g., via stellar winds or supernova explosions. The returned materials are generally enriched in heavy elements, sometimes in the form of dust, and this increases the chemical complexity of galaxies. Stars also change the local physical properties of the ISM, such as the temperature and radiation field. In addition to this evolution due to stellar feedback, the ISM can also accrete mass from the intergalactic medium (IGM) or return material there via galactic outflows. Overall, the ISM is complex and detailed studies of its structure and evolution are needed to understand the star formation process as an integral part of galactic evolution.

## 1.1 Interstellar Medium, Star Formation and Massive Star Formation

The ISM is composed of gas, dust, cosmic rays, radiation fields and magnetic fields. Gas particles in the ISM can exist in ionized, atomic, or molecular form. According to the dominant form of H gas, along with its temperature and density, the ISM can be divided approximately into several different phases, such as the warm neutral medium, cold neutral medium, diffuse molecular gas, and dense molecular gas. As a result of their different local properties, various ways are used to observe them. For example, CO is a common way to trace the dense molecule gas.

Giant Molecular Clouds (GMCs) are massive molecular gas structures, which are likely to be gravitationally bound (e.g. Roman-Duval et al. 2010; Tan et al. 2013b), although often exhibiting supersonic turbulent motions. Typically, GMCs have masses $\gtrsim 10^4 M_\odot$, mean mass surface densities $\Sigma = M/(\pi R^2) \sim 0.02\,\mathrm{g\,cm^{-2}}$ (or $\sim 100 M_\odot\,\mathrm{pc^{-2}}$), and mean volume densities $n_\mathrm{H} \sim 100\,\mathrm{cm^{-2}}$ (McKee & Ostriker 2007; Tan et al. 2013b). GMC radii can be several pc to tens of pc, while their temperatures

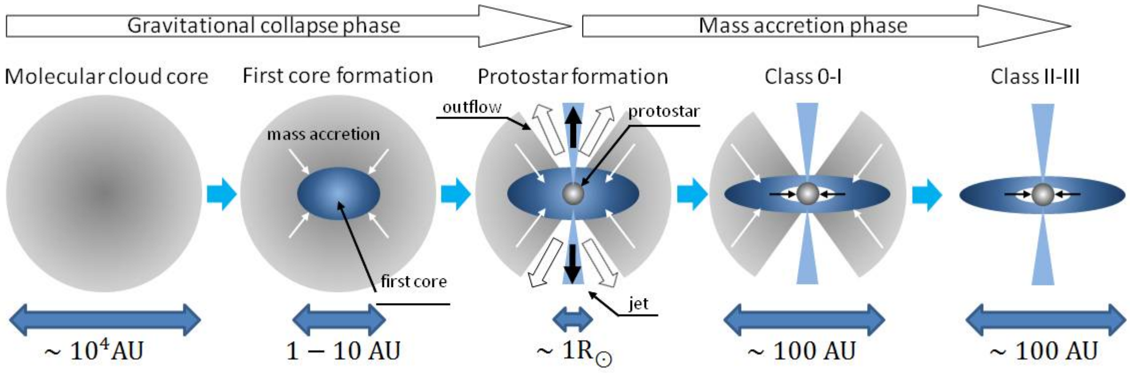

Figure 1.1: Illustration of low-mass star formation by Core Accretion. (Credit: Yusuke Tsukamoto)

are typically in the range from 10-50 K. Most star formation in the Galaxy occurs in GMCs (McKee & Ostriker 2007; Kennicutt & Evans 2012). Substructures also exist in GMCs. The term "clump" is used for a self-gravitating structure which forms a star cluster (Williams et al. 2000). Within the clumps, cores are the smallest units in which star formation occurs (Bergin & Tafalla 2007; Tan et al. 2014). A prestellar core (PSC) is the term given to the core just before it forms a star or small $N$ multiple, with collapse proceeding via a single, central rotationally supported disk. To improve our understanding of the initial conditions of star formation, we need detailed studies of PSCs.

For Sun-like stars, it is believed that their formation involves the following stages with the context of the Core Accretion framework (e.g. Shu et al. 1987; Kennicutt & Evans 2012) (see also Figure 1.1):

- Prestellar Core (PSC): This is a dense, self-gravitating, centrally-concentrated substructure that condenses out of the ambient molecular clump. PSCs typically exhibit infall motions.

- Protostellar Core: Once an approximately hydrostatic star-like structure forms in the center of the core, it is then referred to as a protostellar core. With the contraction of gravity, the temperature reaches 2000 K and dissociates molecular hydrogen, leading to further collapse. The energy coming from gravitational contraction is radiated to warm up the surrounding, infalling envelope gas. This infalling gas, inheriting angular momentum from the PSC, is expected to settle into a rotationally supported accretion disk, although the process depends sensitively on the degree of magnetic coupling and magnetic braking experienced. Magnetic fields threading the accretion disk cause powerful magneto-centrifugally launched outflows to develop, e.g., disk winds, which sweep-up bipolar outflow cavities.

- Young Star and Protoplantary Disk: Eventually the core envelope is either completely accreted or swept away and a remnant protoplanetary disk is left, which is the environment of planet formation.

Massive stars play an important role in the universe because of their strong radiative and mechanical feedback and the heavy metals forged in their cores. However, the formation mechanism of massive stars is still unclear. Candidate theories to explain massive star formation include Turbulent Core Accretion and Competitive Accretion. Turbulent Core Accretion (or the Turbulent Core Model) (McKee & Tan 2003) is a scaled-up version of low-mass star formation theory based on Core Accretion (Shu et al. 1987) (see Figure 1.1). The model proposes that a combination of supersonic turbulence and magnetic fields support massive pre-stellar cores (PSCs) against fragmentation and that these then collapse to a central star-disk system. However, the collapse is not necessarily as ordered as in the case of low-mass star formation, especially if there is significant turbulence in the PSC. The Competitive Accretion model of Bonnell et al. (2001) proposes that large numbers of low-mass stars form in a protocluster clump, with a few of them later accreting chaotically, by Bondi-Hoyle accretion of gas supplied by the collapsing clump, to become massive stars. To distinguish these two theories, one of the decisive differences is in the existence of massive, coherent PSCs.

## 1.2 Virial Theorem

The Virial Theorem is a way to describe the dynamical state of a self-gravitating system, including whether the system is gravitationally bound. From classical mechanics, a system of particles is in virial equilibrium if the kinetic energy $T$ and the gravitational potential energy $U$ satisfy the relationship:

$$2T + U = 0. \tag{1.1}$$

In the case of spherical clouds/clumps/cores of mass $M$ and radius $R$, the internal kinetic energy, $E_k$, is related to the 1-D velocity dispersion, $\sigma$ via $E_k = (3/2)M\sigma^2$. The virial parameter, $\alpha_{\rm vir}$, is defined by

$$\alpha_{\rm vir} = 5\sigma^2 R/(GM) = 2aE_k/E_G, \tag{1.2}$$

where $a$ is the ratio of gravitational energy, $E_G$, to that of a uniform sphere, $3GM^2/(5R)$ (Bertoldi & McKee 1992). The meaning of the virial parameter is the ratio of twice of kinetic energy (estimated by one-dimensional velocity dispersion) to the gravitational energy of uniform sphere. Although astronomical objects are not in practice of uniform density and contain thermal and magnetic field energy, the virial parameter provides a simple way to assess, approximately whether a system is gravitationally bounded ($\alpha_{\rm vir} < 2$). A system is said to be subvirial if $\alpha_{\rm vir} < 1$ and supervirial if $\alpha_{\rm vir} > 1$, although one should remember that the virial equilibrium value of $\alpha_{\rm vir}$ varies depending on the precise internal density structure, degree of elongation, amount of large-scale $B-$field support and intensity of surface pressure.

## 1.3 Magnetic Fields and Mass-to-Flux Ratio

Unlike turbulence, magnetic fields contribute to the pressure support in a gas cloud in a way that cannot be directly seen from the gas motions. For a cloud/clump/core that is threaded by a given magnetic flux, $\Phi$, it will be able to collapse under gravity if its mass is (Mouschovias & Spitzer, L. 1976):

$$M_\Phi = \Phi/(2\pi G^{1/2}). \tag{1.3}$$

The critical ratio of the actual cloud mass to $M_\Phi$ then defines a dimensionless parameter:

$$\mu_\Phi = \frac{M}{M_\Phi} = \frac{2\pi G^{1/2} M}{\Phi} \tag{1.4}$$

If $\mu_\Phi > 1$, then the cloud is magnetically supercritical and the $B-$fields cannot prevent collapse.

# Chapter 2

# Astrochemical Modeling

Astrochemistry is the study of the formation and destruction of chemical species in the universe. One effect of the evolution of the abundances of these species is on the ability of gas to cool by emission of radiation and be heated by absorption of impinging radiation fields. Energy is also directly absorbed and released by endothermic and exothermic chemical reactions, respectively. The ionization fraction of interstellar gas is influenced by its chemistry, and this is important for its coupling to magnetic fields. Line transition radiation from a region is an important diagnostic of different physical conditions, such as density, temperature, radiation fields and ionization rates from cosmic rays, and to better interpret such signals from tracers, such as CO, HCN, $HCO^+$, astrochemical models are necessary.

Currently, several public databases provide a variety of modeling codes to study astrochemistry. Two popular databases are KIDA (Wakelam et al. 2012) and UMIST (McElroy et al. 2013). Associated with these databases, including appending with some additional reactions, several astrochemical codes like Nahoon(Wakelam et al. 2012), AstroChem(Maret & Bergin 2015), Nautilus(Ruaud et al. 2016), UCLCHEM(Holdship et al. 2017) are also publicly available. These codes involve a variety of different model assumptions, especially in the aspect of grain-surface reactions, but generally solve the chemical reactions via coupled rate equations. In this approach, the evolution of species is described by a system of ordinary differential equations. The main difference among these models is then in the diversity and extent of reaction rate networks.

In our work, we will make use primarily of two different chemical models. One is a deuterium fractionation network, which mainly comes from the KIDA database. The other one is a reduced network extracted from the UCLCHEM code, which is a mixture of the UMIST database, augmented by a gas-grain interaction model.

## 2.1 Deuterium Fractionation

According to standard big bang nucleosynthesis theory and WMAP data, the promordial abundance ratio of D/H is $2.37 \times 10^{-5}$ (Spergel 2003). Quasar observations also give results at a similar level ranging from $2 \times 10^{-5}$ to $4 \times 10^{-5}$ (e.g., O'Meara et al. 2001). In contrast, the local ISM value is observed to be slightly lower, i.e.,

$\sim 1.6 \times 10^{-5}$ (Linsky 2007), most likely due to destruction of D via nuclear fusion in stars and recycling of this processed gas back into space via stellar winds, supernovae, etc.

If there is no deuterium fractionation, the D/H fraction in every H-bearing species is thus expected to be about $1.6 \times 10^{-5}$. However, on Earth, in comets or in some observed prestellar cores, the D/H fractions of certain molecules are much higher than this value. For example, the ratio of $N_2D^+$ to $N_2H^+$, which are recognized as good tracers of prestellar cores, has been observed to reach $\gtrsim 0.1$ (Crapsi et al. 2005; Pagani et al. 2007; Miettinen et al. 2012; Kong et al. 2016). These evidences support that deuterium fractionation has occurred by many orders of magnitude. The formed deuterated species could then be inherited by the subsequent protoplantary disk, planetesimals/comets and planets. However, the details of the process by which this may occur are still under debate.

The deuterium fractionation process can be approximately divided into three steps (see Figure 2.1). First is the formation of $H_3^+$, which occurs via the reactions:

$$\begin{aligned} &H_2 + CR \rightarrow H_2^+ + e^- + CR \\ &H_2^+ + H_2 \rightarrow H_3^+ + H \end{aligned} \tag{2.1}$$

Being charged, $H_3^+$ is more reactive than neutral species. The $H_3^+$ then reacts with HD, which is the main reservoir of D atoms, and forms $H_2D^+$.

$$H_3^+ + HD \rightarrow H_2D^+ + H_2 \tag{2.2}$$

The inverse reaction could also happen to destroy $H_2D^+$ to form HD. However, there is a small activation barrier for this inverse reaction. If the temperature is low enough, the environment has a tendency to form $H_2D^+$, which is the beginning of the deuterium fractionation process. $H_2D^+$ then could continue react with HD to form $D_2H^+$ and $D_3^+$.

$$\begin{aligned} &H_2D^+ + HD \rightarrow D_2H^+ + H_2 \\ &D_2H^+ + HD \rightarrow D_3^+ + H_2 \end{aligned} \tag{2.3}$$

The formed $H_2D^+$, $D_2H^+$ and $D_3^+$ may then react with other gas phase species leading to formation of deuterated molecules and molecular ions. Or they may undergo dissociative recombination with electrons to form gas phase D atoms, which may then undergo grain surface reactions to form deuterated ice species.

Since $H_2D^+$ plays a central role in the transfer of D into species and since its abundance increases in cold gas, deuterium fractionation is expected to be enhanced generally in such cold conditions. Furthermore, as the formation of $H_2D^+$ relies on $H_3^+$ as a precursor, it means that an higher cosmic ray ionization rate also accelerates the deuteration process. In addition, as $H_3^+$ is destroyed by O and CO, removing these species from the gas-phase, e.g., by freeze-out onto dust grain ice mantles, also enhances deuterium fractionation. Thus, cold and dense regions of prestellar cores and clumps are ideal places for enhanced deuterium fractionation.

Another important factor influencing deuterium fractionation is the ortho-and-para ratio of molecular hydrogen ($\mathrm{OPR}^{H_2}$). The internal energy of ortho-$H_2$ in

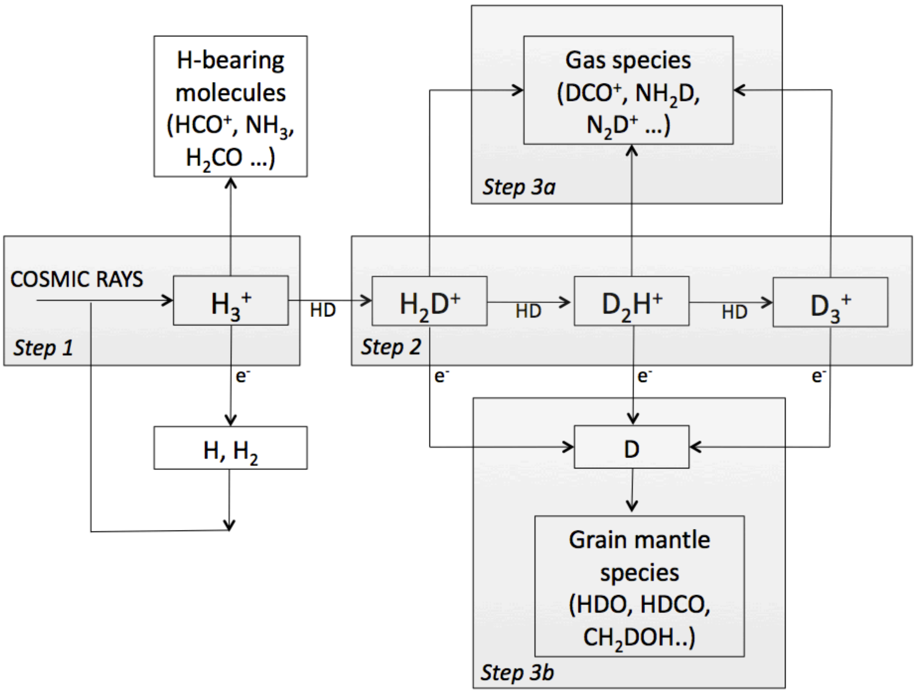
H-bearing molecules (HCO+, NH3, H2CO ...)
Gas species (DCO+, NH2D, N2D+ ...)
Step 3a
COSMIC RAYS
H3+
HD
H2D+
HD
D2H+
HD
D3+
Step 1
Step 2
e-
e-
e-
e-
H, H2
D
Grain mantle species (HDO, HDCO, CH2DOH..)
Step 3b

Figure 2.1: Schematic overview of the processes leading to deuterium fractionation (Credit: Ceccarelli et al. 2014).

its ground state is enough overcome the endothermic energy barrier in the inverse reaction of Equation 2.2 (i.e., $H_2D^+ + H_2 \rightarrow H_3^+ + HD$). As a consequence, the ratio of $H_2D^+/H_3^+$ is suppressed and limits the third step of deuteration. Theoretically, $H_2$ formed on dust grains is expected to have 75% probability to form ortho-$H_2$ and 25% probability to form para-$H_2$.

Subsequently, the ratio decreases over time via reactions with $H^+$ and $H_3^+$ (e.g.: $H^+$+o-$H_2$ → $H^+$+p-$H_2$; p-$H_3^+$+o-$H_2$ → o-$H_3^+$+p-$H_2$) (Hugo et al. 2009; Honvault et al. 2011), especially in cold and dense gas. Due to the low temperature ($\sim$ 20 K), the $\mathrm{OPR}^{\mathrm{H_2}}$ is predicted to be low ($\sim 0.001$) in star-forming environments (e.g., Sipilä et al. 2013; Brünken et al. 2014).

A variety of astrochemical studies have been carried out to model deuterium fractionation. Walmsley et al. (2004) considered a reduced chemical network, including the nuclear spin states of $H_2$, $H_2^+$, $H_3^+$ and $H_2D^+$. This network assumed heavy elements, like C, N, O, etc., are fully depleted. Extending this work, Flower et al. (2006), Hugo et al. (2009), Pagani et al. (2009) and Sipilä et al. (2010) included updated reaction rates for spin states and deuterated forms of $H_2$ and $H_3^+$. Vastel et al. (2012) presented networks including molecular species with up to three atoms. Kong et al. (2015) extended these works to include $H_3O^+$ to acquire more precise results. As a consequence, the abundances of electrons, water, $HCO^+$, $DCO^+$, $N_2H^+$, $N_2D^+$ are improved and have a good agreement with the even more extensive network of Sipilä et al. (2013). More recently, Majumdar et al. (2016), based on the work of Wakelam et al. (2015), presented a complete network including spin state chemistry with 13 elements (H, He, C, N, O, Si, S, Fe, Na, Mg, Cl, P, F). In our work, we have adopted the network from Kong et al. (2015), together with modest improvements suggested by the results of Majumdar et al. (2016).

## 2.2 UCLCHEM

`UCLCHEM` (Holdship et al. 2017) is a time-dependent gas-grain chemical model written in Fortran. It extends the pure gas-phase reactions from the UMIST database with gas-grain interactions, including freeze-out, thermal desorption, photodesorption and cosmic-ray-induced thermal desorption, based on the rate functions of Roberts et al. (2007). To simulate surface chemistry, it adopts an approximated method to allow users to set the branching ratio of freeze-out reactants. For example, when CO sticks on grain mantles, it could be hydrogenated and form $CH_3OH$. `UCLCHEM` allows users to set in a defined grain file that, for example, 90% of CO becomes grain-phase CO and the remaining 10% becomes $CH_3OH$. The whole package also includes a routine to generate the chemical modeling code and other hydrodynamics routines, like C-shocks and evolving conditions of molecular clouds. However, the hydrodynamics modules are limited to single zone or just one dimension.

The standard chemical network defined in `UCLCHEM` includes hundreds of gas-grain reactions, besides 6,173 gas-phase reactions. However, if we only focus on simple species like CO, $H_2O$, etc., a reduced network can provide similar results as the complete network. In our simulations of GMCs, we mainly use the reduced network generated from `UCLCHEM`.

To validate the `UCLCHEM` reduced network, the results are compared with the `UCLCHEM` complete network, as well as the network of Walsh et al. (2015). Note that these two codes include implementations of different grain models, even though both of them use the gas reactions from the UMIST database. For example, `UCLCHEM` is based on Roberts et al. (2007) for implementation of cosmic-ray-induced thermal desorption, while for this Walsh et al. (2015) uses results of Hasegawa et al. (1992). Also, the rate functions are completely different. However, the large uncertainties of the cosmic-ray-induced thermal desorption have been emphasised by Cuppen et al. (2017). In our benchmark tests, these kind of reactions are not included. Furthermore, these two codes use different values of binding energy of ice species. This also leads to significant difference because of the appearance of the binding energy in the exponent in the rate equations. Finally, the values of yields of UV photo reactions are also another source of minor differences. To make the two codes comparable, we synchronize the values of binding energies and yield of UV photo reactions to be consistent with those of Walsh et al. (2015).

Table 2.1 lists the initial abundances used in the benchmark tests. Figures 2.2 and 2.4 show the results of benchmark tests at 10 K and 20 K. Other parameters are fixed to: $n_{\mathrm{H}} = 10^4\ \mathrm{cm}^{-3}$, $A_V = 100$ mag and $\zeta = 1.0 \times 10^{-16}\ \mathrm{s}^{-1}$. The models are evolved for $10^8$ years, which is much longer than the typical free-fall time of GMCs (i.e., $\sim 10^7$ yr). In general, the results of the reduced network are in good agreement with the full network. At 10 K, the difference in abundance of all the species between these two models is smaller than 15%, except for $CH_4$. Although there is a difference

| Species | Abundance ($n_{\mathrm{species}}/n_{\mathrm{H}}$) |
|---|---|
| H | $5.00 \times 10^{-5}$ |
| $H_2$ | 0.500 |
| He | $9.75 \times 10^{-2}$ |
| CO | $1.40 \times 10^{-4}$ |
| N | $7.50 \times 10^{-5}$ |
| O | $1.80 \times 10^{-4}$ |
| Mg | $7.00 \times 10^{-9}$ |
| *Si | $8.00 \times 10^{-9}$ |
| *S | $8.00 \times 10^{-8}$ |
| *Cl | $4.00 \times 10^{-9}$ |
| **GRAIN0 | $2.40 \times 10^{-12}$ |

Table 2.1: The initial abundances of the benchmark tests. (* mark elements ignored in the reduced network; ** marks species, i.e., GRAIN0, only present in the model of Walsh et al. (2015)). There is no explicit abundance of dust grains in `UCLCHEM`; instead those grain-involved reaction rates use some hard coded constants.

of a factor of 13 in the early stages in the abundance of this species, it is not a significant overall problem because of its low abundance. Furthermore, the final difference decreases to be smaller than a factor of 2. At 20 K, the differences are generally larger, but are still smaller than 35% for most species. $CH_4$ still has the largest differences, i.e., a factor of 7.5, but again this does not have a major global impact as it only contains 1% of the total C abundance.

Next we focus on the comparison between the reduced UCLCHEM network and the model of Walsh et al. (2015). At 10 K, the abundance of CO up to about 1 Myr shows a good agreement among the models. However, after this `UCLCHEM` gives the final abundance larger by a factor of 2.58. We see that grain (i.e., ice) phase CO (written as GCO) drops significantly in the Walsh et al. (2015) model after $\sim 10^6$ years (and especially after $2 \times 10^7$ yr, and does not agree well with the results of `UCLCHEM`. The reason for this is that GCO is converted to other species, such as $GCH_4$ and $GC_2H_6$ by surface chemistry, but `UCLCHEM` does not have these kinds of surface reactions. As described above, `UCLCHEM` assigns the fraction of surface species when the freeze-out reactions happen and the species do not convert to each other after this. Other species, i.e., $HCO^+$, HCN, and $CH_4$, generally have relatively good agreement (within a factor of 5) in their abundances, as shown in Figure 2.2.

Figure 2.3(a) shows the evolution of C-bearing species in the Walsh et al. (2015) model at 10 K. As the GCO abundance decreases rapidly in the later stages, the abundances of $GC_2H_6$ and $GC_8H_2$ increase in response. This explains the GCO discrepancy between `UCLCHEM` and the Walsh et al. (2015) model.

In the case of 20 K, the abundance of CO shows larger deviations among the models, with final differences up to a factor of 6.12. As before, most of the differences between `UCLCHEM` and the Walsh et al. (2015) models result from the varying treatment of grain surface reactions, which lead to C being included in $GC_2H_6$ and $GC_8H_2$. The most significant differences between the models, which can be seen in Figure 2.4,

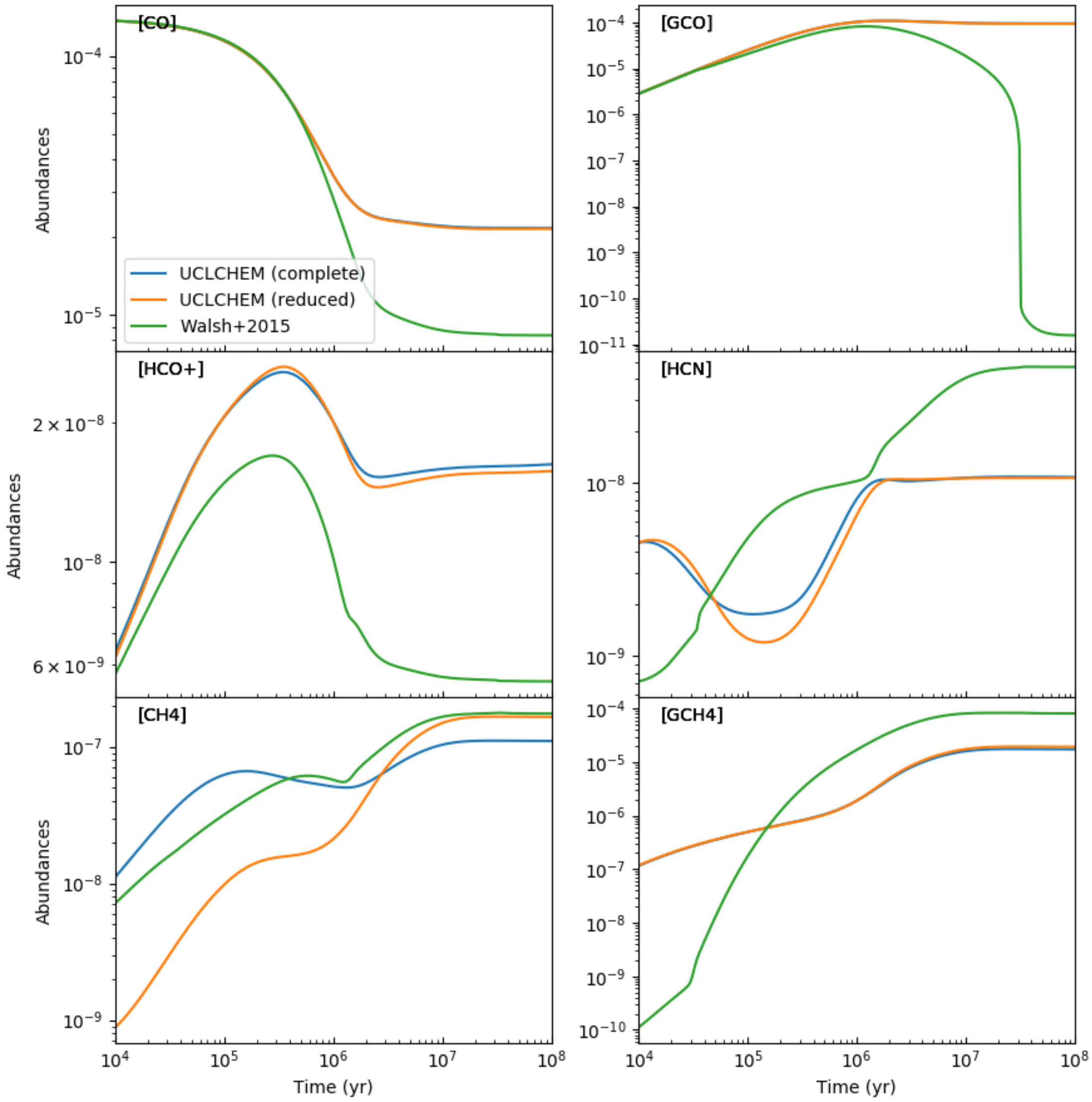

Figure 2.2: Benchmark tests of models of Walsh et al. (2015), full network of `UCLCHEM` and reduced network of `UCLCHEM` at 10 K. The species under comparing are CO, GCO (G: grain-phase), $HCO^+$, HCN, $CH_4$ and $GCH_4$. The name of species is labelled in the top left of each panel.

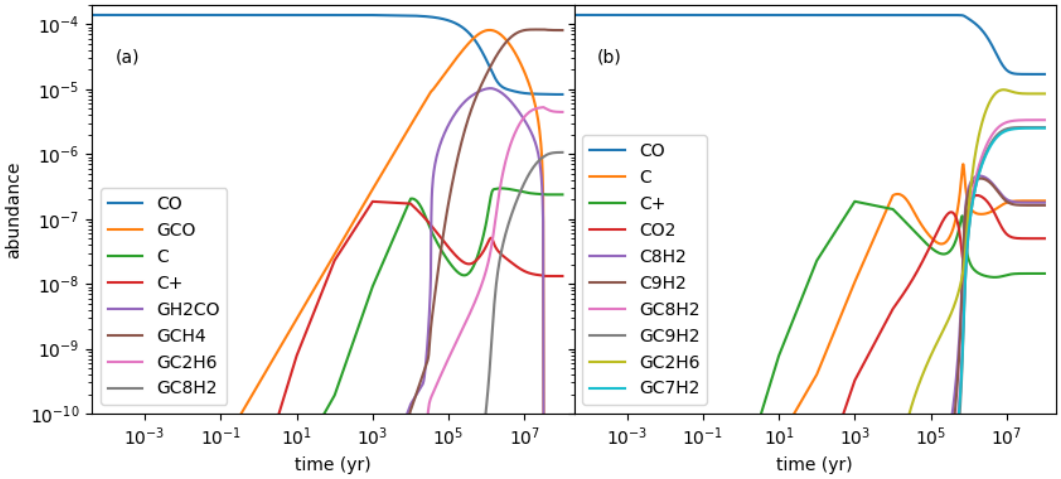

Figure 2.3: The abundance evolution of the most significant C-bearing species in the Walsh et al. (2015) model at 10 K (left) and 20 K (right).

are the abundances of $CH_4$ and $GCH_4$, since `UCLCHEM` does not include longer carbon chains. Thus `UCLCHEM` overpredicts the abundance of methane compared to the Walsh et al. (2015) model. Figure 2.3(b) shows more details of the evolution of the main C-bearing species in the Walsh et al. (2015) model at 20 K. Similar to Figure 2.3(a), $C_2H_6$ and $C_8H_2$ contain a large portion of the C elemental abundance.

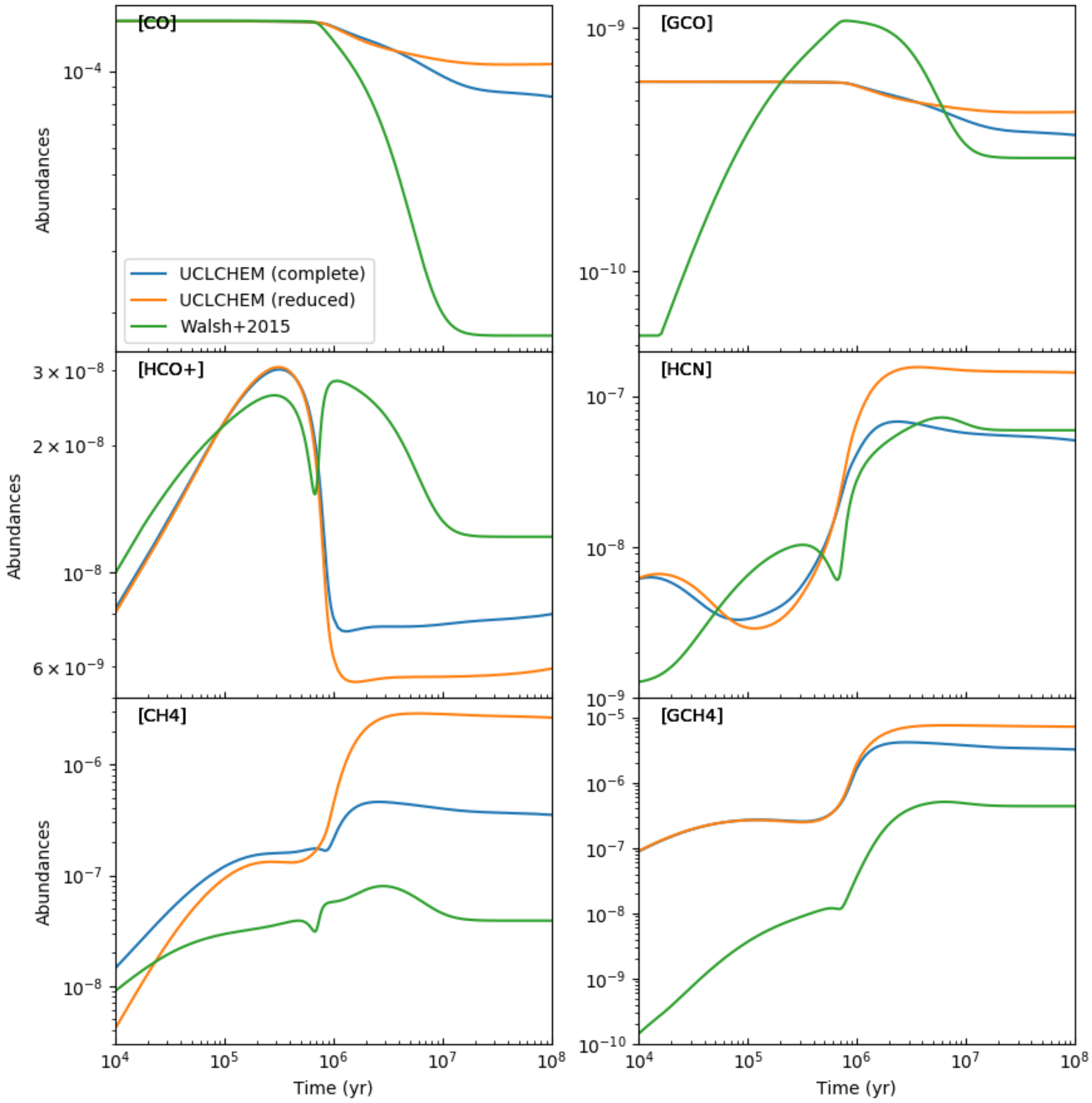

Figure 2.4: Similar to Figure 2.2, except now the benchmark tests are done for 20 K.

# Chapter 3

# Chemodynamics Simulations

Although there are more and more sophisticated astrochemical models, these models are usually implemented in simple single zone, i.e., zero dimensional, or one dimensional frameworks. However, this means that these models typically ignore the influence of kinematic and dynamical effects, especially abundance changes due to advection, including the advective diffusion induced by turbulence. To further understand the influence of such effects, three-dimensional chemodynamics simulations are needed. Previous work on such simulations, of varying levels of complexity, has been presented by several groups (see, e.g., Glover et al. 2010; Bovino et al. 2019; Bellomi et al. 2020).

## 3.1 Coupling Chemistry with Magnetohydrodynamics

In a typical ideal Magnetohydrodynamics (MHD) simulation, the following equations are solved:

$$\begin{aligned}
\frac{\partial \rho}{\partial t} + \boldsymbol{\nabla} \cdot (\rho \mathbf{v}) &= 0, && (3.1)\\
\frac{\partial \rho \mathbf{v}}{\partial t} + \boldsymbol{\nabla} \cdot (\rho \mathbf{v}\mathbf{v} + \mathbf{I}P - \mathbf{B}\mathbf{B}) &= -\rho \boldsymbol{\nabla} \phi, && (3.2)\\
\frac{\partial E}{\partial t} + \boldsymbol{\nabla} \cdot [(E+P)\mathbf{v} - \mathbf{B}(\mathbf{B}\cdot\mathbf{v})] &= -\rho \mathbf{v} \cdot \boldsymbol{\nabla} \phi - \Lambda + \Gamma, && (3.3)\\
\frac{\partial \mathbf{B}}{\partial t} - \boldsymbol{\nabla} \times (\mathbf{v} \times \mathbf{B}) &= 0, && (3.4)
\end{aligned}$$

where $\rho, \mathbf{v}, P, E, \mathbf{B}, \phi$ are the density, velocity vector, pressure, energy density, magnetic field vector and gravitational potential, respectively. Here, $\mathbf{I}$ is an identity tensor, while $\Lambda$ and $\Gamma$ represent the cooling and heating rates, respectively. To include the contributions of magnetic fields, the pressure and energy are given by:

$$P = p + \frac{B^2}{2}, \tag{3.5}$$

$$E = e + \frac{\rho v^2}{2} + \frac{B^2}{2}, \tag{3.6}$$

where $p$ and $e$ are thermal pressure and thermal energy density, respectively. The magnetic permeability ($\mu_0$) is unity in these equations. In the case of ideal gas with a ratio of specific heats $\gamma$, the thermal energy can be expressed as:

$$e = \frac{p}{(\gamma - 1)}. \tag{3.7}$$

If the ideal gas is isothermal, the thermal energy can also be given by sound speed ($c_s$):

$$c_s = \sqrt{\frac{\gamma k T}{\mu m_H}} \tag{3.8}$$

$$e = \frac{\rho c_s^2}{\gamma(\gamma - 1)} \tag{3.9}$$

Equations 3.1 to 3.3 represent the conservation of mass, momentum, and energy, while Equation 3.4 is the magnetic induction equation. However, to extend a fluid to a reactive flow, the equation of species abundance evolution must also be included:

$$\frac{\partial n_i}{\partial t} + \boldsymbol{\nabla} \cdot (n_i \mathbf{v}) - \boldsymbol{\nabla} \cdot (\mathcal{D} \boldsymbol{\nabla} n_i) = C(n_i, n_j, T) - D(n_j, T) n_i, \tag{3.10}$$

where $n_i$ represents the number density of each species and the summation of number density weighted by mass must equal to mass density ($\sum_i n_i m_i = \rho$). This equation includes three processes: advection, diffusion and chemical reactions. The second and the third term on the left-hand side represent the advection and the diffusion processes, respectively. In astrophysical flows, the diffusion term is usually ignored since its influence is much smaller than the advection term. The right-hand side terms refer to the construction ($C$) and destruction ($D$) of $i$th species.

Equation 3.10 can be split into two parts:

$$\frac{\partial n_i}{\partial t} + \boldsymbol{\nabla} \cdot (n_i \mathbf{v}) = 0 \tag{3.11}$$

$$\frac{dn_i}{dt} = C(n_i, n_j, T) - D(n_j, T) n_i \tag{3.12}$$

The first equation only considers the advection term and the second equation solves the reactions, which is the same set of differential equations handled by one-zone astrochemical models (See Chapter 2). That is to say, to implement a chemodynamics simulation, we need to make the hydrodynamics code calculate the advection and then insert the astrochemical model to solve the reactions.

## 3.2 Simulation Code: `ENZO+KROME`

In our projects, we utilize `ENZO` (Bryan et al. 2014) and `KROME` (Grassi et al. 2014) to run our chemodynamics simulations. `ENZO` is a adaptive mesh refinement (AMR) hydrodynamics code, developed originally for cosmological simulations. It has built-in functions using the `GRACKLE` chemistry library to calculate the evolution of primordial gas. `GRACKLE` also supports calculation of heating/cooling rates of primordial gas and metals and some UV background radiation effects. However, the main purpose of `GRACKLE` is primordial chemistry. Although it can be extended to include some user-defined `Cloudy` heating/cooling tables, it is not practical to make it include a general chemical network of the ISM.

Instead, `KROME` is a chemistry package working as a Python-based parser to convert a user-provided chemical network to Fortran codes. Users have the freedom to define their own reaction format by using its pre-defined tokens. It provides a unique interface function so that it can work with other hydrodynamics codes. However, it does not guarantee the consistency with hydrodynamics codes. Users have to ensure that all species in the network exist in the hydrodynamics codes and that the advection is handled by the hydrodynamics codes (see Section 3.1). Besides, because it generates source codes, these codes have to be compiled with the hydrodynamics codes to make the whole combination work. It also provides some official patches for several hydrodynamics codes, including `FLASH, ENZO, GIZMO` and `RAMSES`. For `ENZO`, the patch does not handle advection and the existence of species. Users have to define the additional species and modify some routines for advection and renormalization (e.g., `Grid_SolveHydroEquations.C` for PPM, Zeus, MHD_Li/CT solvers and `Grid_UpdatePrim.C` for Runge-Kutta solvers).

## 3.3 Performance

Although `KROME` provides a way to set up the codes for chemodynamics simulations, a significant problem is the size of the network. To fully model how chemistry happens in the ISM, networks usually contain thousands of reactions. Even if it may only take a few milliseconds to finish one step in one grid cell, the cost becomes significant when there are $10^6$ (the order of $128^3$ resolution) grids. Figure 3.1 shows the mean time of one step of chemodynamics simulations in a $64^3$ domain. The simulations use the same initial condition, but couple with different sizes of networks. We see that the computational time is almost directly proportional to the number of reactions. Note that the performance could also be influenced by the initial conditions. For example, if the temperature of some grids is out of the valid range of reactions, the reaction rates are zeros and could make the calculation faster. However, in general, the performance of simulations can be a thousand times slower than a simulation without chemistry, if a network containing thousands of reactions is used.

Another problem of chemodynamics simulations is the number of species. To track the evolution and calculate the advection, the density of each species must be stored in each grid. As the number of species increases, the simulation also occupies more disk storage and memory. For example, a magnetohydrodynamics

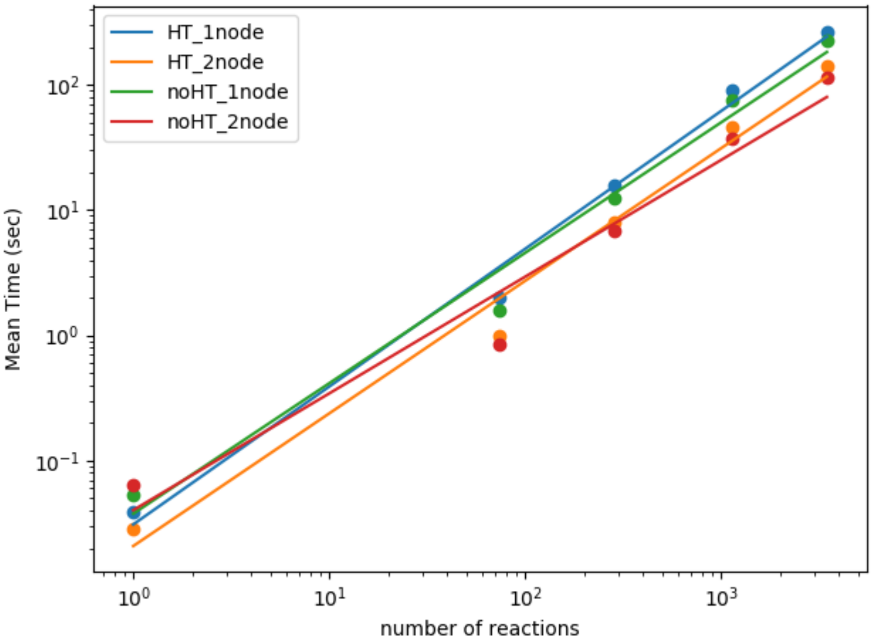

Figure 3.1: Computational time of chemodynamics simulations with different sizes of chemical networks. The same simulation is run with different architectures (HT-with hyper-threading, noHT - without hyper-threading) and different processors (1node - 64 cores, 2node - 128 cores). The test is done on Vera cluster of Chalmers University of Technology in Gothenburg, Sweden (C3SE). The nodes are built with Intel Xeon Gold 6130 CPUs and have 92GB memory on each node.

simulation usually stores about 10 fields (typically, $\rho, \mathbf{v}, E, \mathbf{B}$ and some optional fields like internal energy or gravitational potential). However, an ISM chemical network may contain hundreds of species. For example, if the network contains about 100 species, the simulation with the resolution of $128^3$ will use about 2GB memory. If the resolution is enhanced to $512^2$, the simulation data will exceed 100GB. The number of species limits the resolution and increases the loading of communication when the simulation is running on many CPUs in a cluster.

A simple way to save memory and disk storage is using the AMR structure to limit the finer grids focusing on subregions in the simulation. The way is effective if the interesting regions are only a small portion of the whole domain. However, the side effect is the interpolation error. Although most of the popular AMR codes support high-order interpolation methods and conservative interpolation to reduce numerical errors, element abundance conservation can still be broken (Grassi et al. 2017). The problem is because gradient limiters and interpolation weights can be different for each species. Even if each individual chemical species is conserved during the interpolation, the summation of atoms in species may not be conserved. This means the amount of species should be normalized twice after advection: once for element conservation and once for mass conservation.

However, even if the memory requirement is affordable, the performance problem is still significant. It is impractical to wait over forty days for a simulation originally taking one hour. Several methods can improve the performance:

- Parallelization: Parallelization is a common way to improve the performance of simulations. Currently, `openmp` and `MPI` have been widely applied in numerical codes. `ENZO` also supports the usage of `MPI`, which can accelerate the simulation by requesting more processors from more nodes in a cluster. Figure 3.1 also shows the simulation is almost twice faster by using two nodes rather than one node. However, it is also impractical to offload the heavy computation by requesting hundreds of nodes. Graphics cards could be another choice of parallelization. By using the graphics processing units (GPU) on graphics cards, hydrodynamics simulations could be ten times faster than on a CPU (Schive et al. 2010). Note this also depends on the frequency and the number of units. Usually these kind of tests are done under the same "cost" of a specific cluster. Several studies are working on moving the differential equation solvers onto GPU (Zhou et al. 2011; Niemeyer & Sung 2014; Ahnert et al. 2014; Curtis et al. 2016; Stone et al. 2018). However, these studies are focusing on combustion engineering and biochemistry. They have not been ported to astrochemistry and have several drawbacks. Most solvers are explicit and cannot handle the level of stiffness in astrochemical networks. Some of these solvers use the first order implicit backward differential formula (BDF) method and lose accuracy, while other higher order solvers often have performance problems, e.g., because of their instability and more complex timestep assignments. Astrochemical networks are generally expressed as sparse matrices and if ODE solvers can take advantage of this sparseness, then performance is improved (Grassi et al. 2014). However, most of the GPU-ported solvers assume the matrices are dense and do not take advantage of this feature.

- Reducing the size of network: As the computational load is proportional to the number of reactions, it is intuitive to reduce the load by reducing the number of reactions. This idea has been studied for a long time. It can be done by pre-selecting species and related reactions (Nelson & Langer 1999). Another approach assumes that some species stay with equilibrium abundances to focus on solving the non-equilibrium species (Lam 1993; Glover et al. 2010), where those equilibrium species are chosen by the rapid reaction rates. However, this approach may not be valid for a wide range of parameters because of the variation of reaction rates. A further approach is then to try to dynamically reduce the reactions to avoid this limitation (Tupper 2002; Grassi et al. 2012).

- Reducing the number of chemical time steps: This could be the simplest way to accelerate the simulations, but the method only works when the chemistry timescale is much longer than the hydrodynamics timestep. If the hydrodynamics timestep is much shorter than the chemistry timescale, the chemistry calculation can be operated only every several hydrodynamics timesteps and keep a relatively good approximation for the abundances. This approach has been implemented in our `ENZO` codes. However, if the simulation is undergoing fast heating/cooling, this approach will lose accuracy.

- Neural network: Due to the advance of deep learning, neural networks have become a popular tool in a variety of fields. As the fundamental neural network, artificial neural networks also have been widely applied in computational chemistry, biochemistry, etc. (Goncalves et al. 2013). A recent work also applies the method to create an emulator of `UCLCHEM` (De Mijolla et al. 2019). As a black box, the emulator skips the cost of solving differential equations, but reproduces, approximately, the nonlinear results. The problem becomes how to train a valid model and guarantee the correctness over a wide range of parameter space and whether there is a general way to train an effective model.

# Chapter 4

# Introduction to Paper

## 4.1 Paper I

In this paper, we focus on the deuterium fractionation in massive prestellar cores. The reason is that $N_2H^+$ and its deuterated form $N_2D^+$ have been observed in several prestellar cores and are thought to be good diagnostic tracers of these objects (Caselli et al. 2002; Tan et al. 2013a; Kong et al. 2016). The cold and dense gas is also an ideal place for deuterium fractionation (see Section 2.1). The emission lines of these species are thus also useful to interpret the kinematics in the cores. As a follow-up work of (Goodson et al. 2016), we also use the chemical network of (Kong et al. 2015), but with minor updates from (Majumdar et al. 2016). The network contains species composed by heavy elements, C, N, and O, and we investigate the influence of depletion factors of these species. We then use `ENZO` and `KROME` to couple the chemical network with a magnetohydrodynamics simulation of a massive prestellar core.

We focus on the influences of chemical parameters to a particular prestellar core. The initial conditions of the prestellar core are fixed to mass $= 60\ M_\odot$, mass surface density $= 0.3\ \mathrm{g\,cm^{-2}}$, radius $= 0.1$ pc. The free-fall time is then 76 kyr. The prestellar core also has a turbulent velocity field and a cylindrically symmetric magnetic field to make the core slightly supervirial in the beginning. Since there is no driving of the turbulent velocity field, the core will begin to collapse as turbulence decays. The chemical parameters we study are the initial $\mathrm{OPR}^{\mathrm{H_2}}$, temperature, cosmic-ray ionization rate and depletion factor of CO and N (two factors, one controlling the abundances of C and O, another one controlling the abundance of N) and the initial chemical age, i.e., affecting initial abundances.

We follow the chemical evolution in the core for 0.8 free-fall times and analyze the number densities and column densities of $N_2H^+$ and $N_2D^+$. Figure 4.1 shows the comparison of abundances with observational data. We conclude that one model with high cosmic-ray ionization rate ($1.0 \times 10^{-16}\mathrm{s^{-1}}$) and high depletion factor ($f_D^{\mathrm{CO}} = 1000$, $f_D^{\mathrm{N}} = 100$) is one of the best models for matching observational data of massive PSCs. The abundances also allow us to estimate the velocity gradient, the velocity dispersion, the rotational energy, the kinetic energy and the virial parameter of the simulated core as would be traced under the assumption of optical thin

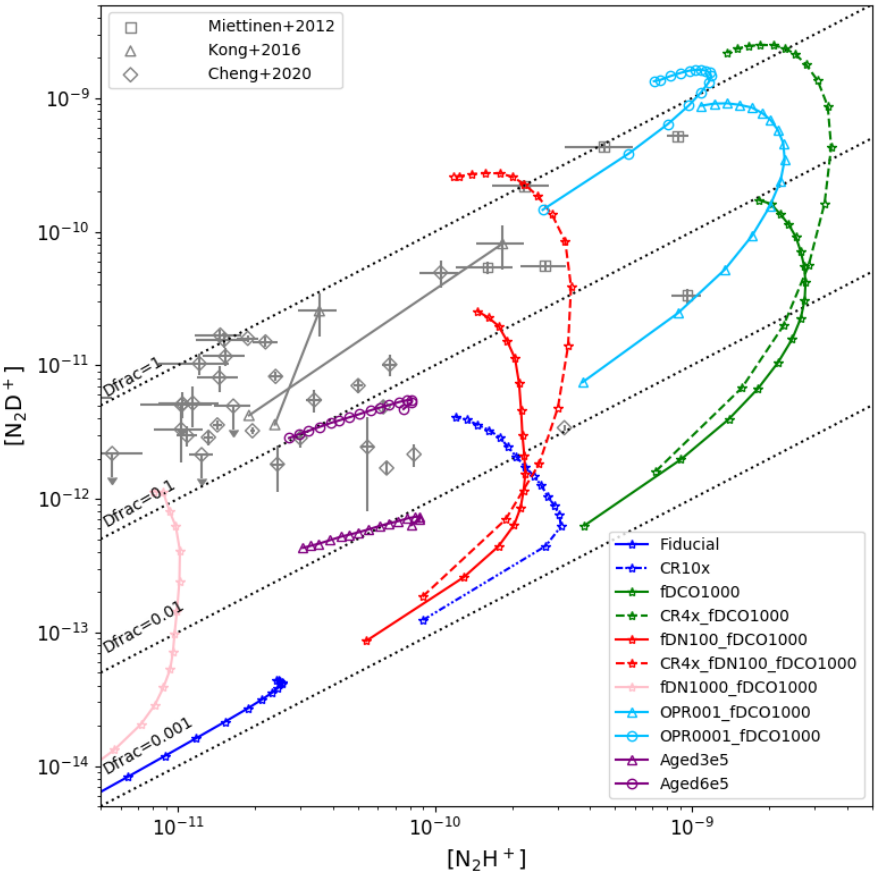

Figure 4.1: Time evolution of the average abundances of $N_2H^+$ and $N_2D^+$ in massive PSC simulations, as listed in the lower right legend. The grey squares, triangles and diamonds are observational data from Miettinen et al. (2012), Kong et al. (2016), and Cheng et al. (2021).

emission of $N_2D^+$(3-2). Overall, the rotational energy is small compared with the gravitational energy. The core can appear subvirial in certain directions during much of the evolution because of the contribution of magnetic fields to its support.

Although we found one possible way for the prestellar core to reach an high deuterium fraction, comparable with some observed systems, the fast collapse rate may also influence the results. For example, if the prestellar core had stronger $B-$field support and collapsed more slowly, then a lower cosmic ray ionization rate would likely be allowed to enable a similar level of deuteration to be reached.

# Chapter 5

# Outlook and Future Work

## 5.1 Ambipolar Diffusion in Massive PSCs

Following the work done in Paper I, we now include the non-ideal MHD effect of ambipolar diffusion (AD) into the simulation. If ambipolar diffusion is considered, the prestellar core is able to contract starting from a stronger initial $B-$field condition, although taking a longer time to collapse (see, e.g., the models of Hennebelle et al. 2020; Zhao et al. 2020; Machida & Basu 2020, for the case of AD in low-mass cores, including its influence on disk formation). Thus, such models are likely to be able to achieve a given level of deuteration with a lower cosmic-ray ionization rate. Also, their kinematics are likely to show much small degrees of turbulence, since this tends to decay after about one free-fall time.

Figure 5.1 shows the average mean molecular weight of the ionised species (excluding electrons), $\mu_i$ (in units of the proton mass), in some of the core simulations of Paper I. As expected, it shows that $\mu_i$ decreases as the CO and N depletion factors increase, i.e., a larger fraction of the charge is carried by light species, such as $H_3^+$ and $H_2D^+$.

The ambipolar diffusion time $\tau_{\rm AD}$ can be approximated as:

$$\tau_{\rm AD} \sim \frac{8\pi L^2}{B^2} n_n n_i < \sigma v > \frac{\mu_n \mu_i}{\mu_n + \mu_i} \qquad (5.1)$$

where $n_n$, $n_i$ and $\mu_n$ are the number density of neutral particles, the number density of ion particles and the mean molecular mass of neutral particles, respectively. $< \sigma v >$ is the ion-neutral collisional rate coefficient, which has a value $\sim 10^{-9}$ cm$^3$ s$^{-1}$. Since $n_i \ll n_n$, $\mu_n$ can be approximated to 2.33 for all models. We use the values of the initial radius and the initial magnetic field strength at the core boundary for the length scale, $L$, and average magnetic field strength, $B$, to estimate the ambipolar diffusion time.

The positive ion abundances of some of the prestellar cores in Paper I are plotted in Figure 5.2. Then, Figure 5.3 shows $\tau_{\rm AD}$ estimates based on the average ion mean molecular weight and abundances in the models. The figure shows that the AD time is sensitive to the cosmic-ray ionization rate and depletion factor and thus

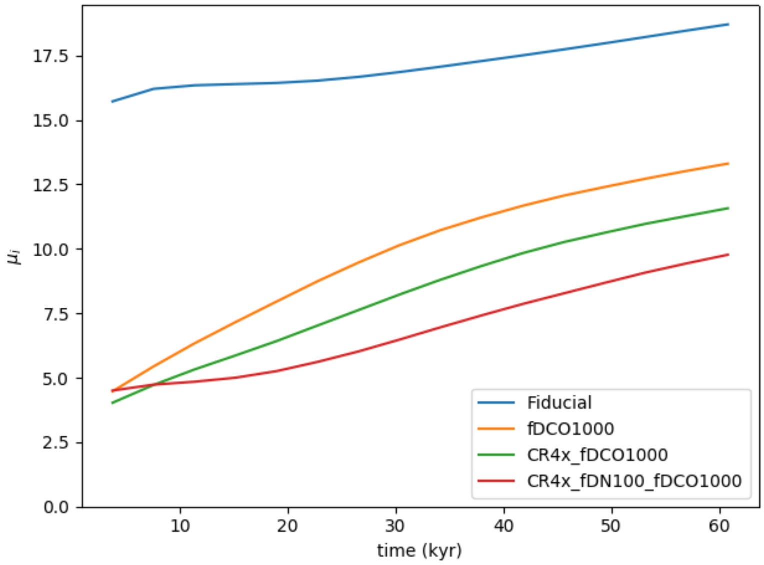

Figure 5.1: Time evolution of the mean molecular weight of ionised species (excluding electrons), $\mu_i$, in some of the core simulations of Paper I.

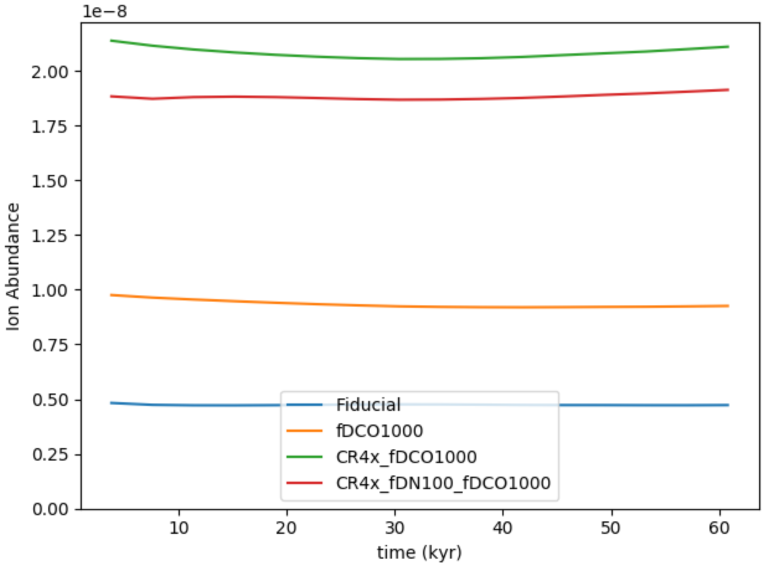

Figure 5.2: The positive ion abundances of several simulated PSCs of Paper I (see text).

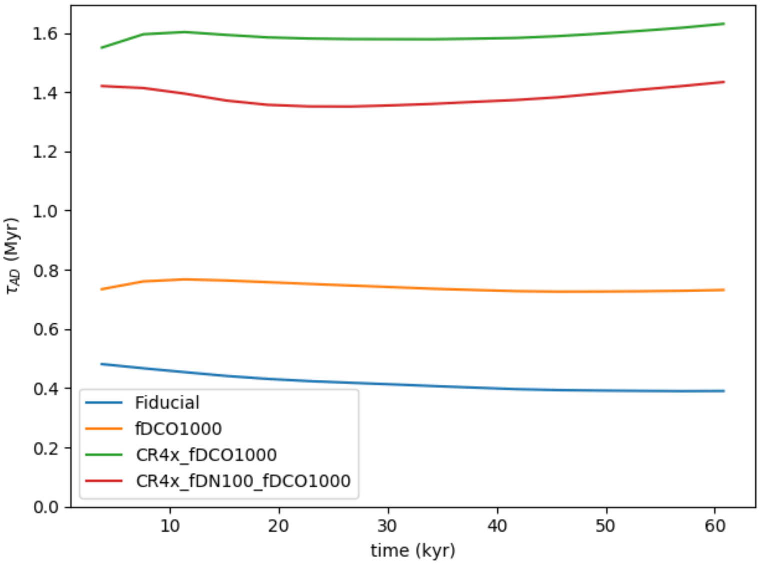

Figure 5.3: Estimates of the evolution of ambipolar diffusion time of several simulated PSCs of Paper I (see text).

astrochemical effects can have an important impact on the physical evolution of star formation from strongly magnetised molecular clouds.

We have implemented ambipolar diffusion in our PSC simulations following the method described in Christie et al. (2017). Although the fiducial table of resistivities of Christie et al. (2017) is based on different species and a PDR astrochemical model, it is still instructive to know how significantly ambipolar diffusion influences the collapse. Figure 5.4 shows the mass-weighted mass surface density distribution function of the fiducial model in Paper I and the corresponding results with ambipolar diffusion at 0.6 free-fall time. The mass fractions where the mass surface density $> 3.0\,\mathrm{g\,cm^{-2}}$ in the case with AD are 0.244, 0.282, 0.197 in x, y, and z viewing directions, respectively. In the case without AD, the mass fractions are 0.211, 0.211, 0.113. Thus we see there is modest enhancements in the amounts of dense gas when AD is accounted for. However, in this supercritical case, the magnetic field is relatively weak and in general the effects of AD are quite modest. Much larger differences are expected to arise in PSCs in which the initial magnetic field is stronger such that the initial PSC is magnetically subcritical. Indeed, in such circumstances, collapse would only be able to proceed in the model with ambipolar diffusion and its rate is likely to be sensitive to details of the astrochemistry.

Figure 5.5 shows a scatter plot of deuterium fraction versus density in the simulations with and without AD. At $0.25t_{\mathrm{ff}}$, the deuterium fraction still has a good agreement between the simulations, but the model with ambipolar diffusion has a slightly wider distribution in its low-density region. Again, because these models have relatively weak $B-$fields and are undergoing relatively fast collapse, the particular influence of AD on the chemical properties is minimal. Larger differences are likely to arise during the evolution of more strongly magnetised cores.

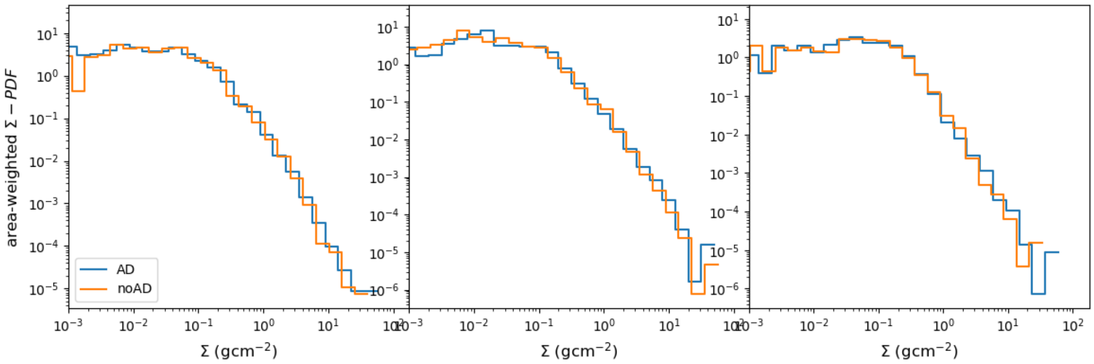

Figure 5.4: Probability distribution functions of mass surface density at $t = 0.6t_{\mathrm{ff}}$. AD - with ambipolar diffusion, noAD - without ambipolar diffusion.

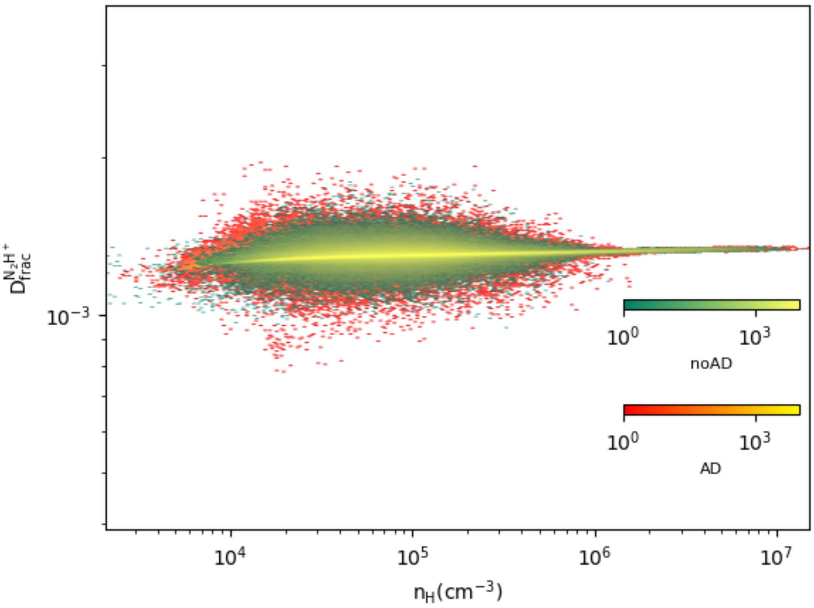

Figure 5.5: Scatter plot of density and deuterium fraction in core at $t = 0.25t_{\mathrm{ff}}$.

## 5.2 Cloud-Cloud Collisions

Giant Molecular Cloud (GMC) collisions are proposed to be an important mechanism to create dense gas concentrations and thus trigger star formation. Wu et al. (2015) and Wu et al. (2017) have used `ENZO` and `GRACKLE` to study collisions of magnetised, turbulent GMCs, utilising heating and cooling rates based on photon dissociation region (PDR) models that estimate the chemical composition of such clouds and their envelopes. The PDR model also allows the prediction of molecular lines, such as higher $J$ CO lines, e.g., CO(8-7), which can be important diagnostics of warm, dense gas created in the collisions. However, these simulations do not dynamically couple chemistry and hydrodynamics and so their predictions have significant uncertainties.

We have coupled the fiducial GMC-GMC collision simulation of Wu et al. (2017), i.e., involving two identical GMCs colliding at 10 km $s^{-1}$, with the reduced `UCLCHEM` astrochemical network (see Section 2.2) to improve the accuracy of the abundance estimates of CO, as well as those of other species that probe various conditions, such as dense gas (e.g., HCN, $HCO^+$) and the lower density envelopes (e.g., $C^+$). Since gas-grain interactions are also supported by the network, this will also allow us to study the gas-phase depletion due freeze-out in dense, cold gas. The results can be use to improve the modeling of the initial conditions of the prestellar core simulation, i.e., to assess how massive PSCs arise from realistic GMC conditions.

To couple the reduced network with the original cloud collision simulation, we again incorporate `KROME` with `ENZO`. `GRACKLE` is used to follow heating and cooling, but still based on the Wu et al. (2015) tabulated rates based on their PDR model. Visual extinction, $A_V$, which is required by our astrochemical network, is specified by the density-extinction relation described in Wu et al. (2015), i.e., to be consistent with the PDR model. The initial abundances are given by Table 2.1, i.e., the same as the benchmark tests presented in Section 2.

Figure 5.6 shows the snapshot of the fiducial GMC-GMC collision simulation at 1 Myr. The streamlines indicate the direction and magnitude of magnetic fields. In Figure 5.7, the time evolution of mass surface density, $C^+$ column density, and CO column density in the colliding clouds are plotted. Although C is in CO in the beginning, the molecule is destroyed almost immediately and produces $C^+$ after about 10,000 years because of the relatively low density. This is consistent with the results of the single grid model shown in Figure 5.8, which has $n_{\mathrm{H}} = 100\,\mathrm{cm}^{-3}$, $T = 10\,\mathrm{K}$, $\zeta = 1.0 \times 10^{-16}\,\mathrm{s}^{-1}$, and FUV field strength of $4G_0$. As the clouds are colliding into each other, the growth of density and visual extinction make CO formation easier. Thus, although the abundances are still relatively low at this stage ($\lesssim 10^{-7}$), they are on a trend of increasing quite rapidly and CO is expected to soon become the dominant reservoir of C in the dense clumps.

## 5.3 Porting astrochemical tools onto GPUs

The performance of astrochemical simulations has been discussed in Section 3.3. To run a huge network at high resolution, improving the performance is needed. So far, because the chemical networks are much slower than hydrodynamics, we have

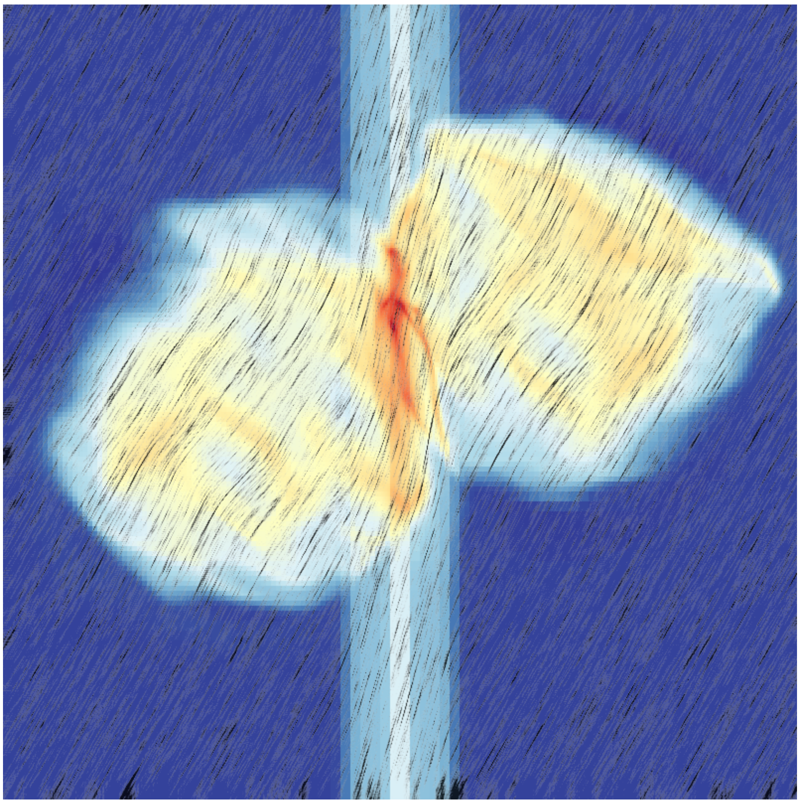

Figure 5.6: The mass surface density of colliding clouds at 1 Myr in a box of 128 pc$^3$. The streamlines indicate the strength of the magnetic field.

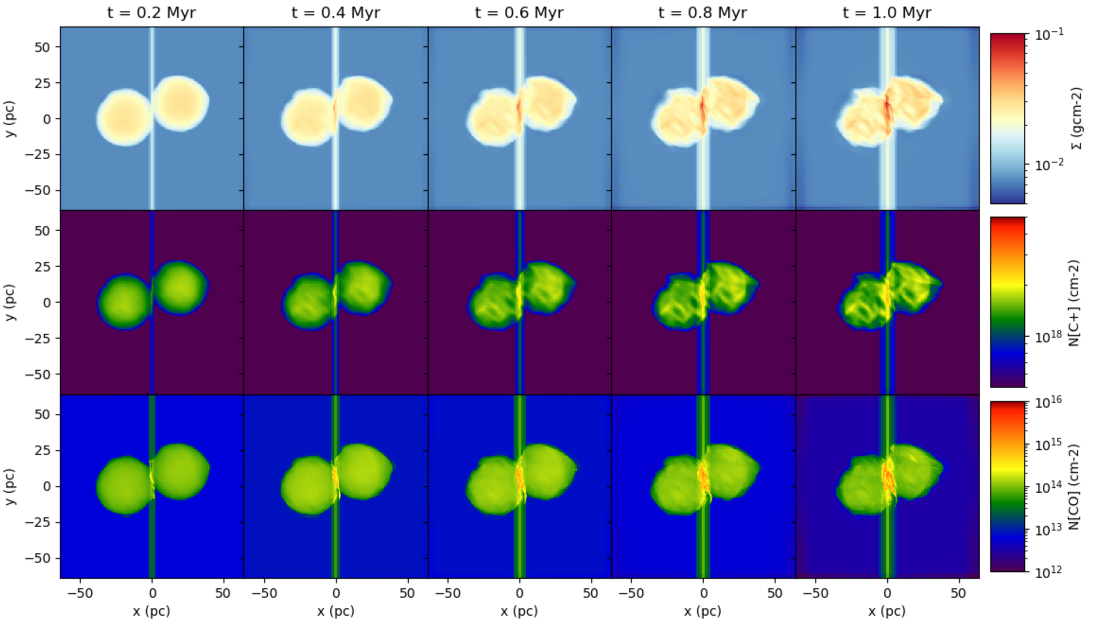

Figure 5.7: Time evolution of the colliding clouds. The columns from left to right shows the snapshots every 200 kyr. The rows from top to bottom are: mass surface density, C$^+$ column density, and CO column density. Each box is 128 pc on a side.

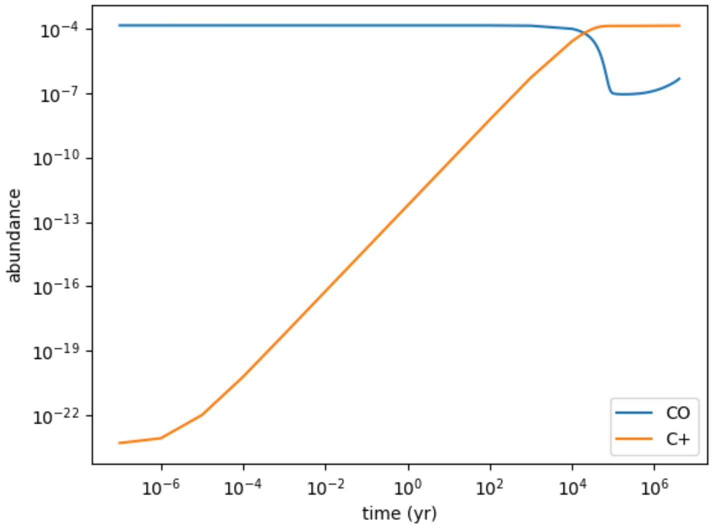

Figure 5.8: The chemical evolution of top abundant C-bearing species in single grid model run with `UCLCHEM`.

used ways of reducing the number of chemical cycles to accelerate the simulation. However, to further improve the performance, we aim to have an high-order implicit ODE solver executable on GPUs. We first plan to port the available `lsoda` GPU solver to fit the requirement of astrochemistry. `lsode` is another solver that has been widely used and takes advantage of the sparsity of matrix, but it is written in Fortran77. Porting it onto GPU is another potential future project.

# Bibliography

Ahnert, K., D. Demidov, & M. Mulansky (2014). "Solving ordinary differential equations on GPUs". In: *Numerical Computations with GPUs*, pp. 125–157. ISBN: 9783319065489. DOI: `10.1007/978-3-319-06548-9_7` (cit. on p. 19).

Bellomi, E., B. Godard, P. Hennebelle, V. Valdivia, G. P. des Forêts, P. Lesaffre, & M. Pérault (2020). *3D chemical structure of diffuse turbulent ISM. I. Statistics of the HI-to-H2 transition.* arXiv: `2009.05466` (cit. on p. 15).

Bergin, E. A. & M. Tafalla (2007). "Cold Dark Clouds: The Initial Conditions for Star Formation". In: *Annual Review of Astronomy and Astrophysics* 45.1, pp. 339–396. ISSN: 0066-4146. DOI: `10.1146/annurev.astro.45.071206.100404`. arXiv: `0705.3765` (cit. on p. 4).

Bertoldi, F. & C. F. McKee (Aug. 1992). "Pressure-confined clumps in magnetized molecular clouds". In: *The Astrophysical Journal* 395, p. 140. ISSN: 0004-637X. DOI: `10.1086/171638` (cit. on p. 5).

Bonnell, I. A., M. R. Bate, C. J. Clarke, & J. E. Pringle (2001). "Competitive accretion in embedded stellar clusters". In: *Monthly Notices of the Royal Astronomical Society* 323.4, pp. 785–794. ISSN: 00358711. DOI: `10.1046/j.1365-8711.2001.04270.x`. arXiv: `0102074 [astro-ph]` (cit. on p. 5).

Bovino, S., S. Ferrada-Chamorro, A. Lupi, G. Sabatini, A. Giannetti, & D. R. G. Schleicher (2019). "The 3D Structure of CO Depletion in High-mass Prestellar Regions". In: *The Astrophysical Journal* 887.2, p. 224. ISSN: 1538-4357. DOI: `10.3847/1538-4357/ab53e4`. arXiv: `1910.13981` (cit. on p. 15).

Brünken, S. et al. (2014). "H2D+ observations give an age of at least one million years for a cloud core forming Sun-like stars". In: *Nature* 516.7530, pp. 219–221. ISSN: 14764687. DOI: `10.1038/nature13924` (cit. on p. 9).

Bryan, G. L. et al. (2014). "Enzo: An adaptive mesh refinement code for astrophysics". In: *Astrophysical Journal, Supplement Series* 211.2. ISSN: 00670049. DOI: `10.1088/0067-0049/211/2/19` (cit. on p. 17).

Caselli, P., C. M. Walmsley, A. Zucconi, M. Tafalla, L. Dore, & P. C. Myers (2002). "Molecular Ions in L1544. I. Kinematics". In: *The Astrophysical Journal* 565.1, pp. 331–343. ISSN: 0004-637X. DOI: `10.1086/324301`. arXiv: `0109021 [astro-ph]` (cit. on p. 21).

Ceccarelli, C., P. Caselli, D. Bockelee-Morvan, O. Mousis, S. Pizzarello, F. Robert, & D. Semenov (Mar. 2014). "Deuterium Fractionation: the Ariadne's Thread from the Pre-collapse Phase to Meteorites and Comets today". In: DOI: `10.2458/azu_uapress_9780816531240-ch037`. arXiv: `1403.7143` (cit. on p. 9).

Cheng, Y., J. C. Tan, P. Caselli, L. Fissel, H. G. Arce, F. Fontani, M. D. Goodson, M. Liu, & N. Galitzki (Jan. 2021). “Star Formation in a Strongly Magnetized Cloud”. In: *arXiv e-prints*, arXiv:2101.01326, arXiv:2101.01326. arXiv: `2101.01326 [astro-ph.GA]` (cit. on p. 22).

Christie, D., B. Wu, & J. C. Tan (2017). “GMC Collisions as Triggers of Star Formation. IV. The Role of Ambipolar Diffusion”. In: *The Astrophysical Journal* 848.1, p. 50. ISSN: 1538-4357. DOI: `10.3847/1538-4357/aa8a99`. arXiv: `1706.07032` (cit. on p. 25).

Crapsi, A., P. Caselli, C. M. Walmsley, P. C. Myers, M. Tafalla, C. W. Lee, & T. L. Bourke (2005). “ Probing the Evolutionary Status of Starless Cores through N 2 H + and N 2 D + Observations ”. In: *The Astrophysical Journal* 619.1, pp. 379–406. ISSN: 0004-637X. DOI: `10.1086/426472` (cit. on p. 8).

Cuppen, H. M., C. Walsh, T. Lamberts, D. Semenov, R. T. Garrod, E. M. Penteado, & S. Ioppolo (2017). “Grain Surface Models and Data for Astrochemistry”. In: *Space Science Reviews* 212.1-2, pp. 1–58. ISSN: 15729672. DOI: `10.1007/s11214-016-0319-3` (cit. on p. 10).

Curtis, N. J., K. E. Niemeyer, & C.-J. Sung (July 2016). “An investigation of GPU-based stiff chemical kinetics integration methods”. In: *Combustion and Flame* 179, pp. 312–324. ISSN: 15562921. DOI: `10.1016/j.combustflame.2017.02.005`. arXiv: `1607.03884` (cit. on p. 19).

De Mijolla, D., S. Viti, J. Holdship, I. Manolopoulou, & J. Yates (2019). “Incorporating astrochemistry into molecular line modelling via emulation”. In: *Astronomy and Astrophysics* 630. ISSN: 14320746. DOI: `10.1051/0004-6361/201935973`. arXiv: `1907.07472` (cit. on p. 20).

Flower, D. R., G. Pineau Des Forêts, & C. M. Walmsley (2006). “The importance of the ortho:para H 2 ratio for the deuteration of molecules during pre-protostellar collapse”. In: *Astronomy and Astrophysics* 449.2, pp. 621–629. ISSN: 00046361. DOI: `10.1051/0004-6361:20054246`. arXiv: `0601429 [astro-ph]` (cit. on p. 9).

Glover, S. C. O., C. Federrath, M. M. Low, & R. S. Klessen (2010). “Modelling CO formation in the turbulent interstellar medium 1 I N T RO D U C T I O N”. In: 29, pp. 2–29. DOI: `10.1111/j.1365-2966.2009.15718.x` (cit. on pp. 15, 19).

Goncalves, V., K. Maria, & A. B. F. da Silv (Jan. 2013). “Applications of Artificial Neural Networks in Chemical Problems”. In: *Artificial Neural Networks - Architectures and Applications*. InTech. DOI: `10.5772/51275` (cit. on p. 20).

Goodson, M. D., S. Kong, J. C. Tan, F. Heitsch, & P. Caselli (Sept. 2016). “Structure, Dynamics and Deuterium Fractionation of Massive Pre-Stellar Cores”. In: *The Astrophysical Journal* 833.2, p. 274. ISSN: 1538-4357. DOI: `10.3847/1538-4357/833/2/274`. arXiv: `1609.07107` (cit. on p. 21).

Grassi, T., S. Bovino, T. Haugbølle, & D. R. G. Schleicher (Apr. 2017). “A detailed framework to incorporate dust in hydrodynamical simulations”. In: *Monthly Notices of the Royal Astronomical Society* 466.2, pp. 1259–1274. ISSN: 0035-8711. DOI: `10.1093/mnras/stw2871`. arXiv: `1606.01229` (cit. on p. 18).

Grassi, T., S. Bovino, D. R. Schleicher, J. Prieto, D. Seifried, E. Simoncini, & F. A. Gianturco (2014). “KROME-a package to embed chemistry in astrophysical simulations". In: *Monthly Notices of the Royal Astronomical Society* 439.3, pp. 2386–2419. ISSN: 13652966. DOI: `10.1093/mnras/stu114` (cit. on pp. 17, 19).

Grassi, T., S. Bovino, F. A. Gianturco, P. Baiocchi, & E. Merlin (Sept. 2012). "Complexity reduction of astrochemical networks". In: *Monthly Notices of the Royal Astronomical Society* 425.2, pp. 1332–1340. ISSN: 00358711. DOI: `10.1111/j.1365-2966.2012.21537.x` (cit. on p. 19).

Hasegawa, T. I., E. Herbst, & C. M. Leukng (1992). "Models of gas-grain chemistry in dense interstellar clouds with complex organic molecules". In: *The Astrophysical Journal Supplement Series* 82, p. 167. ISSN: 0067-0049. DOI: `10.1086/191713` (cit. on p. 10).

Hennebelle, P., B. Commerçon, Y. N. Lee, & S. Charnoz (2020). "What determines the formation and characteristics of protoplanetary discs?" In: *arXiv* 67, pp. 1–18. ISSN: 23318422 (cit. on p. 23).

Holdship, J., S. Viti, I. Jiménez-Serra, A. Makrymallis, & F. Priestley (2017). "UCLCHEM: A Gas-grain Chemical Code for Clouds, Cores, and C-Shocks". In: *The Astronomical Journal* 154.1, p. 38. ISSN: 0004-6256. DOI: `10.3847/1538-3881/aa773f` (cit. on pp. 7, 10).

Honvault, P., M. Jorfi, T. González-Lezana, A. Faure, & L. Pagani (2011). "Ortho-para H2 conversion by proton exchange at low temperature: An accurate quantum mechanical study". In: *Physical Review Letters* 107.2, pp. 1–4. ISSN: 10797114. DOI: `10.1103/PhysRevLett.107.023201` (cit. on p. 9).

Hugo, E., O. Asvany, & S. Schlemmer (2009). "H3+ + H2 isotopic system at low temperatures: Microcanonical model and experimental study". In: *Journal of Chemical Physics* 130.16. ISSN: 00219606. DOI: `10.1063/1.3089422` (cit. on p. 9).

Kennicutt, R. C. & N. J. Evans (2012). *Star formation in the milky way and nearby galaxies.* DOI: `10.1146/annurev-astro-081811-125610`. arXiv: `1204.3552` (cit. on p. 4).

Kong, S., P. Caselli, J. C. Tan, V. Wakelam, & O. Sipilä (May 2015). "THE DEUTERIUM FRACTIONATION TIMESCALE IN DENSE CLOUD CORES: A PARAMETER SPACE EXPLORATION". In: *The Astrophysical Journal* 804.2, p. 98. ISSN: 1538-4357. DOI: `10.1088/0004-637X/804/2/98`. arXiv: `1312.0971v5` (cit. on pp. 9, 10, 21).

Kong, S., J. C. Tan, P. Caselli, F. Fontani, T. Pillai, M. J. Butler, Y. Shimajiri, F. Nakamura, & T. Sakai (2016). "the Deuterium Fraction in Massive Starless Cores and Dynamical Implications". In: *The Astrophysical Journal* 821.2, p. 94. ISSN: 1538-4357. DOI: `10.3847/0004-637x/821/2/94`. arXiv: `1509.08684` (cit. on pp. 8, 21, 22).

Lam, S. H. (Mar. 1993). "Using CSP to Understand Complex Chemical Kinetics". In: *Combustion Science and Technology* 89.5-6, pp. 375–404. ISSN: 0010-2202. DOI: `10.1080/00102209308924120` (cit. on p. 19).

Linsky, J. L. (2007). "D/H and nearby interstellar cloud structures". In: *Space Science Reviews.* Vol. 130. 1-4, pp. 367–375. DOI: `10.1007/s11214-007-9160-z` (cit. on p. 8).

Machida, M. N. & S. Basu (May 2020). "Different modes of star formation - II. Gas accretion phase of initially subcritical star-forming clouds". In: *Monthly Notices of* *the Royal Astronomical Society* 494.1, pp. 827–845. DOI: `10.1093/mnras/staa672`. arXiv: `2003.03078 [astro-ph.SR]` (cit. on p. 23).

Majumdar, L., P. Gratier, M. Ruaud, V. Wakelam, C. Vastel, O. Sipilä, F. Hersant, A. Dutrey, & S. Guilloteau (2016). "Chemistry of TMC-1 with multiply deuterated species and spin chemistry of H 2 , H 2 + , H 3 + and their isotopologues". In: *Monthly Notices of the Royal Astronomical Society* 4479, stw3360. ISSN: 0035-8711. DOI: `10.1093/mnras/stw3360` (cit. on pp. 9, 10, 21).

Maret, S. & E. A. Bergin (July 2015). *Astrochem: Abundances of chemical species in the interstellar medium.* ascl: `1507.010` (cit. on p. 7).

McElroy, D., C. Walsh, A. J. Markwick, M. A. Cordiner, K. Smith, & T. J. Millar (2013). "The UMIST database for astrochemistry 2012". In: 36, pp. 1–13 (cit. on p. 7).

McKee, C. F. & E. C. Ostriker (2007). "Theory of Star Formation". In: *Annual Review of Astronomy and Astrophysics* 45.1, pp. 565–687. ISSN: 0066-4146. DOI: `10.1146/annurev.astro.45.051806.110602`. arXiv: `0707.3514` (cit. on pp. 3, 4).

McKee, C. F. & J. C. Tan (Mar. 2003). "The Formation of Massive Stars from Turbulent Cores". In: *The Astrophysical Journal* 585.2, pp. 850–871. ISSN: 0004-637X. DOI: `10.1086/346149` (cit. on p. 5).

Miettinen, O., J. Harju, L. K. Haikala, & M. Juvela (2012). "A (sub)millimetre study of dense cores in Orion B9". In: *Astronomy and Astrophysics* 538, pp. 1–20. ISSN: 00046361. DOI: `10.1051/0004-6361/201117849` (cit. on pp. 8, 22).

Mouschovias, T. C. & J. Spitzer, L. (1976). "Note on the collapse of magnetic interstellar clouds". In: *Astrophysical Journal* 210, pp. 326, 327 (cit. on p. 6).

Nelson, R. P. & W. D. Langer (Oct. 1999). "On the Stability and Evolution of Isolated Bok Globules". In: *The Astrophysical Journal* 524.2, pp. 923–946. ISSN: 0004-637X. DOI: `10.1086/307823` (cit. on p. 19).

Niemeyer, K. E. & C. J. Sung (2014). "Accelerating moderately stiff chemical kinetics in reactive-flow simulations using GPUs". In: *Journal of Computational Physics* 256, pp. 854–871. ISSN: 00219991. DOI: `10.1016/j.jcp.2013.09.025`. arXiv: `1309.2710` (cit. on p. 19).

O'Meara, J. M., D. Tytler, D. Kirkman, N. Suzuki, J. X. Prochaska, D. Lubin, & A. M. Wolfe (May 2001). "The Deuterium to Hydrogen Abundance Ratio toward a Fourth QSO: HS 0105+1619". In: *The Astrophysical Journal* 552.2, pp. 718–730. ISSN: 0004-637X. DOI: `10.1086/320579` (cit. on p. 7).

Pagani, L., C. Vastel, E. Hugo, V. Kokoouline, C. H. Greene, A. Bacmann, E. Bayet, C. Ceccarelli, R. Peng, & S. Schlemmer (2009). "Chemical modeling of L183 (L134N): An estimate of the ortho/para H 2 ratio". In: *Astronomy and Astrophysics* 494.2, pp. 623–636. ISSN: 00046361. DOI: `10.1051/0004-6361:200810587`. arXiv: `0810.1861` (cit. on p. 9).

Pagani, L., A. Bacmann, S. Cabrit, & C. Vastel (2007). "Depletion and low gas temperature in the L183 (=L134N) prestellar core: The N2H+-N2D+ tool". In: *Astronomy and Astrophysics* 467.1, pp. 179–186. ISSN: 00046361. DOI: `10.1051/0004-6361:20066670` (cit. on p. 8).

Roberts, J. F., J. M. Rawlings, S. Viti, & D. A. Williams (2007). "Desorption from interstellar ices". In: *Monthly Notices of the Royal Astronomical Society* 382.2, pp. 733–742. ISSN: 00358711. DOI: `10.1111/j.1365-2966.2007.12402.x` (cit. on p. 10).

Roman-Duval, J., J. M. Jackson, M. Heyer, J. Rathborne, & R. Simon (2010). "Physical properties and galactic distribution of molecular clouds identified in the galactic ring survey". In: *Astrophysical Journal* 723.1, pp. 492–507. ISSN: 15384357. DOI: `10.1088/0004-637X/723/1/492`. arXiv: `1010.2798` (cit. on p. 3).

Ruaud, M., V. Wakelam, & F. Hersant (2016). "Gas and grain chemical composition in cold cores as predicted by the Nautilus three-phase model". In: *Monthly Notices of the Royal Astronomical Society* 459.4, pp. 3756–3767. ISSN: 13652966. DOI: `10.1093/mnras/stw887`. arXiv: `1604.05216` (cit. on p. 7).

Schive, H. Y., Y. C. Tsai, & T. Chiueh (2010). "Gamer: A graphic processing unit accelerated adaptive-mesh-refinement code for astrophysics". In: *Astrophysical Journal, Supplement Series* 186.2, pp. 457–484. ISSN: 00670049. DOI: `10.1088/0067-0049/186/2/457`. arXiv: `0907.3390` (cit. on p. 19).

Shu, F. H., F. C. Adams, & S. Lizano (Sept. 1987). "Star Formation in Molecular Clouds: Observation and Theory". In: *Annual Review of Astronomy and Astrophysics* 25.1, pp. 23–81. ISSN: 0066-4146. DOI: `10.1146/annurev.aa.25.090187.000323` (cit. on pp. 4, 5).

Sipilä, O., P. Caselli, & J. Harju (2013). "HD depletion in starless cores". In: *Astronomy and Astrophysics* 554, pp. 1–14. ISSN: 00046361. DOI: `10.1051/0004-6361/201220922`. arXiv: `1304.4031` (cit. on p. 9).

Sipilä, O., E. Hugo, J. Harju, O. Asvany, M. Juvela, & S. Schlemmer (2010). "Modelling line emission of deuterated H3+ from prestellar cores". In: *Astronomy and Astrophysics* 509.1. ISSN: 14320746. DOI: `10.1051/0004-6361/200913350`. arXiv: `0911.1236` (cit. on p. 9).

Spergel, D. et al (2003). "First-Year WMAP Observations: Determination of Cosmological Parameters". In: *The Astrophysical Journal Supplement Series* 148, pp. 175–194 (cit. on p. 7).

Stone, C. P., A. T. Alferman, & K. E. Niemeyer (2018). "Accelerating finite-rate chemical kinetics with coprocessors : Comparing vectorization methods on GPUs , MICs , and CPUs". In: *Computer Physics Communications*. ISSN: 0010-4655. DOI: `10.1016/j.cpc.2018.01.015` (cit. on p. 19).

Tan, J. C., M. T. Beltran, P. Caselli, F. Fontani, A. Fuente, M. R. Krumholz, C. F. McKee, & A. Stolte (Feb. 2014). "Massive Star Formation". In: *International Astronomical Union Colloquium* 140, pp. 176–184. ISSN: 0252-9211. DOI: `10.2458/azu_uapress_9780816531240-ch007`. arXiv: `1402.0919` (cit. on p. 4).

Tan, J. C., S. Kong, M. J. Butler, P. Caselli, & F. Fontani (2013a). "The dynamics of massive starless cores with alma". In: *Astrophysical Journal* 779.2. ISSN: 15384357. DOI: `10.1088/0004-637X/779/2/96` (cit. on p. 21).

Tan, J. C., S. N. Shaske, & S. Van Loo (Mar. 2013b). "Molecular Clouds: Internal Properties, Turbulence, Star Formation and Feedback". In: *Proceedings of the International Astronomical Union* 8.S292, pp. 19–28. ISSN: 1743-9213. DOI: `10.1017/S1743921313000173` (cit. on p. 3).

Tupper, P. F. (2002). “ADAPTIVE MODEL REDUCTION FOR CHEMICAL KINETICS”. In: 42.2, pp. 447–465 (cit. on p. 19).

Vastel, C., P. Caselli, C. Ceccarelli, A. Bacmann, D. C. Lis, E. Caux, C. Codella, J. A. Beckwith, & T. Ridley (2012). “Upper limit for the D 2H + ortho-to-para ratio in the prestellar core 16293E (CHESS)”. In: *Astronomy and Astrophysics* 547, pp. 1–7. ISSN: 00046361. DOI: `10.1051/0004-6361/201219616`. arXiv: `1210.0804` (cit. on p. 9).

Wakelam, V. et al. (2012). “A kinetic database for astrochemistry (KIDA)”. In: *Astrophysical Journal, Supplement Series* 199.1. ISSN: 00670049. DOI: `10.1088/0067-0049/199/1/21`. arXiv: `1201.5887` (cit. on p. 7).

Wakelam, V. et al. (2015). “The 2014 kida network for interstellar chemistry”. In: *Astrophysical Journal, Supplement Series* 217.2, p. 20. ISSN: 00670049. DOI: `10.1088/0067-0049/217/2/20`. arXiv: `1503.01594` (cit. on p. 9).

Walmsley, C. M., D. R. Flower, & G. P. D. Forets (2004). “Complete Depletion in prestellar cores”. In: *Astronomy and Astrophysics* 418.0718, p. 22. ISSN: 0004-6361. DOI: `10.1051/0004-6361:20035718;`. arXiv: `0402493 [astro-ph]` (cit. on p. 9).

Walsh, C., H. Nomura, & E. Van Dishoeck (2015). “The molecular composition of the planet-forming regions of protoplanetary disks across the luminosity regime”. In: *Astronomy and Astrophysics* 582, pp. 1–28. ISSN: 14320746. DOI: `10.1051/0004-6361/201526751` (cit. on pp. 10–13).

Williams, J. P., L. Blitz, & C. F. McKee (Feb. 2000). “The Structure and Evolution of Molecular Clouds: from Clumps to Cores to the IMF”. In: pp. 97–120. arXiv: `9902246 [astro-ph]` (cit. on p. 4).

Wu, B., S. V. Loo, J. C. Tan, & S. Bruderer (2015). “GMC COLLISIONS AS TRIGGERS of STAR FORMATION. I. PARAMETER SPACE EXPLORATION with 2D SIMULATIONS”. In: *Astrophysical Journal* 811.1, p. 56. ISSN: 15384357. DOI: `10.1088/0004-637X/811/1/56` (cit. on p. 27).

Wu, B., J. C. Tan, F. Nakamura, S. V. Loo, D. Christie, & D. Collins (2017). “GMC Collisions as Triggers of Star Formation. II. 3D Turbulent, Magnetized Simulations”. In: *The Astrophysical Journal* 835.2, p. 137. ISSN: 1538-4357. DOI: `10.3847/1538-4357/835/2/137` (cit. on p. 27).

Zhao, B., P. Caselli, Z.-Y. Li, R. Krasnopolsky, H. Shang, & K. H. Lam (Sept. 2020). “The Interplay between Ambipolar Diffusion and Hall Effect on Magnetic Field Decoupling and Protostellar Disc Formation”. In: *arXiv e-prints*, arXiv:2009.07820, arXiv:2009.07820. arXiv: `2009.07820 [astro-ph.SR]` (cit. on p. 23).

Zhou, Y., J. Liepe, X. Sheng, M. P. Stumpf, & C. Barnes (2011). “GPU accelerated biochemical network simulation”. In: *Bioinformatics* 27.6, pp. 874–876. ISSN: 13674803. DOI: `10.1093/bioinformatics/btr015` (cit. on p. 19).

# Part II

# Appended papers

# Paper 1

# Deuterium Chemodynamics of Massive Pre-stellar Cores

Chia-Jung Hsu, Jonathan C. Tan, Matthew D. Goodson, Paola Caselli, Bastian Körtgen, Yu Cheng

*Accepted by MNRAS*